Numerical simulation and engineering-geological assessment of a creeping slope in the Alps

Zur Erlangung des akademischen Grades eines Doktors der Naturwissenschaften an der Fakultät für Bauingenieur-, Geo- und Umweltwissenschaften der Universität Karlsruhe (TH) genehmigte

DISSERTATION

von
Geeralt van den Ham
aus Buren (die Niederlande)

2006

Tag der mündlichen Prüfung: 10.02.2006
Referent: Prof. Dr. Dr. K. Czurda
Korreferent: Prof. Dr. E. Fecker

Acknowledgements

This thesis is the final result of a PhD-research that was carried out at the Department of Applied Geology of the University of Karlsruhe. In the first place I would like to thank my promotor Prof. Dr. Kurt Czurda for giving me the opportunity to work on this research topic and for his stimulating help and assistance.
I further would like to thank Prof. Dr. Edwin Fecker of the University of Tübingen, who was willing to become my co-promotor at a late stage of this research.

This study was performed in the framework of the Postgraduate Programme 'Natural Disasters', which is facilitated by the German Research Foundation DFG. The DFG is gratefully acknowledged for the financial support.

I would like to express my special thanks to Joachim Rohn for introducing me into the fieldwork area and for the very fruitful discussions throughout the entire research. I am also very grateful to Thomas Meier and Roberto Cudmani of the Institute of Soil and Rock Mechanics for providing the material models and giving me very useful advices concerning the soil mechanical part of this study.

I would like to thank all my colleagues of the Department of Applied Geology, of which over the years many became friends, especially André, Matthias, Roland, Heidi and Mitsch. They made the years I spent in Karlsruhe to a very pleasant and important period of my life.

If working abroad, the knowledge of having people that can bolster you in times things look less positive is very important. Therefore I would like to thank my Dutch friends Wouter, Michael, Mees and Propser. I am also very grateful to Henk, Trijnie and Arnout for their patience and understanding they have shown over the years and for being always there for me.
Finally I would like to express my very specials thanks to Martha, not only for her great help in the preparation of this thesis, but also for her enormous moral support.

Table of contents

Chapter 1 General introduction

1.1 Introduction

In mountainous areas landslides are one of the most detrimental natural hazards. Increasing population pressure in many Alpine regions has resulted in an increased friction between demand for land and the risk on landslides. For this reason, research after the triggers of landslides and the behaviour of landslides is of utmost importance. Much research has focused on fast landslides, as these are traditionally considered to be most detrimental, whereas much less attention is paid to slow slope movements. However, although slow slope movements, or creep movements, are obviously less spectacular, they may form a considerable burden for the maintenance of infrastructure and buildings on or below the slope. Furthermore, creep movements may also represent an initial stage of fast landslides or earth flows with even more detrimental impact. Hence, it is important to be able to understand the mechanisms by which large slopes gradually move downhill and to be able to simulate their actual displacements and velocities. This way infrastructure and built-up area can be planned while taking into account the slow moving slopes, whereas the more dangerous, fast landslides can be predicted in an earlier stage.

Slow creep movements are typical for soils built in cohesive soils, which can be described, from a geological view, as soils characterised by a high clay content (the soil mechanical definition is given below). In the Alps many slopes in cohesive soils exist, which in most cases have developed due to in-situ weathering of the original bedrock or they represent glacial deposits.

As prediction of creep movements concerns the prediction of both displacements and velocities as well as their evolution over time, conventional limit equilibrium analysis is meaningless, as this method only calculates a static state of the slope. Furthermore, only critical states along (pre-defined) slip planes are considered, whereas creep may also occur beyond the critical state. Numerical models, on the other hand, can be a useful tool, provided that an appropriate constitutive law is used that describes the material behaviour in an accurate way. Application of the Finite Element method allows, in contrary to the limit equilibrium method, simulation of continuous fields of displacements, which in reality is observed in many creeping slopes.

From a soil mechanical view, cohesive soil materials can be defined as materials that can creep (i.e. strain rate≠0 and stress rate=0), relaxate (i.e. strain rate=0 and stress rate≠0) and that must be rate-dependent (i.e. stress evolution and stiffness depend on strain rate). Therefore, the model should be based on a material law that describes these phenomena. In literature many studies involving numerical simulations of creeping slopes using elastoplastic and elasto-viscoplastic equations can be found (e.g. Cristescu et al., 2002, Desai et al., 1995, Samtami et al., 1996 and Vulliet and Hutter, 1998). For the viscous part of deformation most of these studies use Bingham, Newton or Norton creep laws. Many of these material laws, however, turn out not to be able to describe all of these phenomena accurately. Furthermore, they often are very complicated, in the sense that determination of the material parameters and calibration cannot always be performed with standard laboratory tests on soil samples.

During the last decade more and more visco-hypoplastic material models have been used, which are an alternative for material models based on the elastoviscoplastic laws. Similar to the elastoviscoplastic laws they are phenomenological, but they have the advantage that material parameters can all be determined with standard laboratory tests and are strictly separated from state variables (stress and density). Up to now the visco-hypoplastic law, in the version of the University of Karlsruhe (Niemunis, 2003), has been validated for many different geotechnical problems (e.g. calculation of slope deformations due to open pit mining (Karcher, 2003)). However, application to a large-size creeping slope has not been done before.

1.2 Aims of the study

The objective of this thesis is to show the applicability of the visco-hypoplastic material law, in the version of Niemunis (2003), for prediction of the creep movements of a known large-size natural slope. The method used involves (a) determination of parameters of the material law based on laboratory tests on soil samples taken from the slope (b) numerical simulation of the laboratory tests in order to test the validity of the material law for the soils studied and (c) testing the material model on the slope by back-predicting measured creep movements by means of two different numerical programmes.

1.3 Approach

One of the major problems in the modelling of geotechnical problems in general is the limited availability of subsurface data, e.g. material distribution, the magnitude and distribution of stresses, densities and pore water pressures, but also slope geometry. The larger the slope to be simulated, the less likely it is that the available subsurface data cover the entire variability of above mentioned parameters and variables within the slope. Even when detailed data are available at some locations on the slope (e.g. boreholes), the possibility to incorporate such detailed information into a model is limited as it is not known to what extent such detailed information applies to the rest of the slope. Simulation of a large-size slope, therefore, requires a different approach compared to small-sized slopes. The limited possibility of sampling the full extent of the slope has to be compensated with engineering geological knowledge and expertise. Samples, on which material parameters are determined by means of laboratory testing, cannot be taken randomly from the slope but have to be carefully chosen, based on the genesis of the slope materials and slope history. Similarly, if measurements concerning the actual stress state or density are lacking, these have to be estimated (or simulated) based on geological and slope historical knowledge.

Prediction of displacements and velocities by means of simulation is always based on simplifications and assumptions, which may result in a reduction of the model performance. Simplifications concern (a) an approximation of initial and boundary conditions (e.g. the distribution of initial stresses and densities, pore water pressure distribution and slope geometry), (b) the assumption that the field measurements sufficiently capture the spatial heterogeneity of the slope (e.g. that the selected samples sufficiently represent the slope materials) and (c) the discretisation of continuous variables (e.g. the homogenisation of microscopic heterogeneities, such as thin layers observed in borehole records, into larger homogeneous units). With increasing slope size and/or heterogeneity or decreasing density of subsurface data, these simplifications become stronger. In order to assess the impact of these simplifications on the predictive quality of the model, in this study a sensitivity analysis was carried out, in which the unknown parameters and variables are varied between expected ranges.

This study focuses on the methods of predicting creep movements rather than the prediction of the exact displacements and velocities themselves. It is shown that the problem of simulation of a large-size deforming slope can only be tackled using a combination of a proper constitutive material model on the one hand and (engineering) geological knowledge to compensate the limited availability of subsurface data, on which the model has to be based, on the other hand. Furthermore, the predictive value of simulation results can only be judged if both the fundamentals of the used material model and the geology and material characteristics of the slope studied are well understood.

1.4 Framework

This thesis consists of two parts. In the first part the theoretical background of the physical processes on a microscopic scale, which determine the overall behaviour of slow moving slopes in cohesive materials, is given (chapter 2). Secondly the fundamentals of the visco-hypoplastic material model, which describes the time-dependent stress-strain behaviour of cohesive soils, and determination of the material parameters are discussed. Also methods for dealing with material heterogeneity by means of homogenisation and assessment of the initial state variables are discussed (chapter 3). In the second part of this thesis it is shown how the visco-hypoplastic law was applied on a natural creeping slope in the Upper-Austrian Alps by means of numerical simulations. Chapter 4 describes the general methods used and gives an introduction to the study area, including its geological setting. In chapter 5 slope history is described chronologically and a detailed characterisation of the slope materials is given as well as the results of on-site geotechnical measurements that were conducted. These form the basis for the design of the models with which slope movements were simulated and which are subject of chapter 6. Besides the methods of development of the models, which includes determination of material parameters and initial state variables, this chapter shows the results of the simulations and a number of sensitivity analyses.

Chapter 7 finally summarises and discusses the outcomes of this study. Conclusions are drawn concerning the suitability of the applied approach and the visco-hypoplastic material law for predicting slow moving slopes.

Part 1 Theory

Chapter 2 The mechanical behaviour of cohesive soils on a microscopic scale

2.1 Introduction

Subject of this thesis are gravity-driven, slow slope movements as a result of the viscous properties of cohesive and saturated soil materials. In the chapter 3 as well as in the case study, which will be described in Part 2, slope deformations will be approached on a macroscopic scale, i.e. a scale on which the time-dependent stress-strain behaviour of a *volume* of soil is considered. This means that the various properties associated with discrete soil entities (i.e. grains and clay particles) are integrated and averaged to the level of a homogeneous continuum model (Prevost and Popescu, 1996). As the overall mechanical behaviour of the soil is determined by its microscopic properties, these are described in this chapter.

2.2 Properties of cohesive soils on a microscopic scale

Soil material is an assemblage of solid, fluid and gaseous components. The solid particles are represented by sand and silt grains as well as clay particles. The pores in between them are filled with free and bonded pore water and air or other gases.
While in cohesionless soils (i.e. granular soils) the stress-strain behaviour is mainly determined by granulometry of the particles, in cohesive soils (i.e. soils mainly composed of clay particles) it is predominantly determined by (complex) physical-chemical effects. As this thesis focuses on cohesive soils, in the following an overview of these effects is given, as well as their influence on the time-dependent stress-strain behaviour of the soil.

Due to their crystalline structure the surfaces of clay particles have a negative electrical charge (which can be a result of isomorphous substitution, shortage of cations in the crystal sheets or absorption of anions at the rupture planes of broken crystalline structures). In a clay suspension (i.e. the clay is surrounded by water), this negative charge is neutralised by attraction of dissolved cations (for example Na^+ or Ca^{2+} from dissolved salts in the pore water) and water dipoles of the free pore water (hydrated water). Directly on the crystal surface only cations are bonded, which remain immobilised due to strong attractive forces. This layer of cations, called stern layer, has a

thickness between 2,5 Å and 10 Å (=10^{-10} m) (Mitchell, 1993). Up to the stern layer follows a diffuse layer of cations and hydrated water molecules, which' concentration is decreasing exponentially outwards (Fig. 2.1).

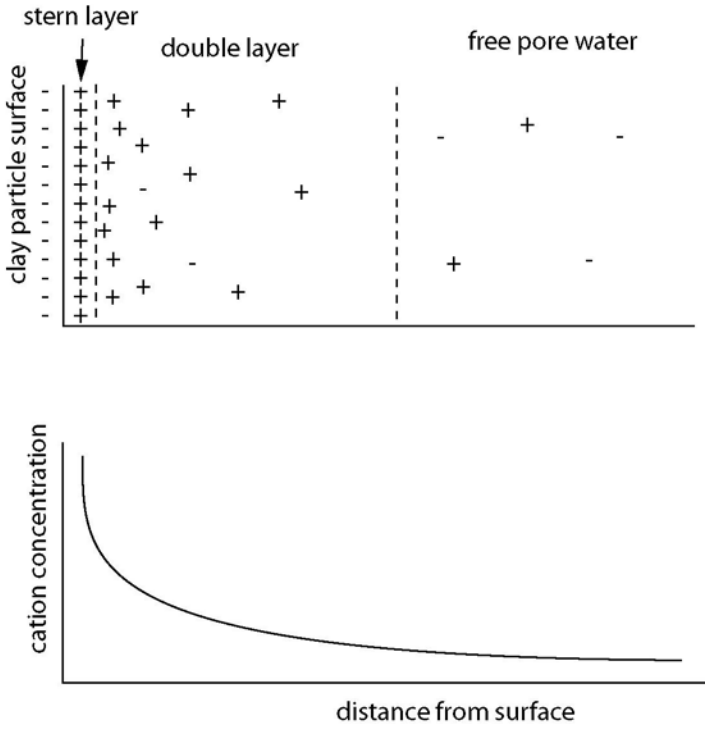

Fig. 2.1. Ion distribution (+ and - depict a cation and anion respectively) in the vicinity of a clay particle (after Mitchell, 1993).

This layer, called (electrical) double layer or layer of adsorbed water, reaches to the point in which the electrolyte concentration of the free pore water has been reached. Due to Brownian motions a permanent exchange of cations takes place between the double layer and the free pore water. On the one hand the cations and water dipoles tend to diffuse into the free pore water, on the other hand they are attracted towards the charged clay particle surface. The thickness of the double layer depends on the electrolyte concentration of the free pore water, the valence and size of the exchangeable cations, temperature and the acidity (pH) of the pore water. An increase of the electrolyte concentration in the free pore water as well as the exchange of cations by cations of a higher valence and/or smaller size lead to a reduction of the thickness of the double layer. The thickness is further reduced by an increase of temperature, although this effect is rather small (Mitchell, 1993), and by a decrease of pH of the pore water.

Due to the high attractive forces between the cations and water dipoles, absorbed water has (dependent on the electrolyte concentration) an up to two times higher density compared to the free pore water. Because the mobility of the cations in the double layer is reduced, absorbed water has a higher viscosity (Krieg, 2000). The volumetric content of absorbed water depends on the specific surface of the soil material. Due to their small size and platy shape clay particles have a very high specific surface, varying from 5 $m^2 \cdot g^{-1}$ (e.g. kaolinite clays) up to 800 $m^2 \cdot g^{-1}$ (e.g. montmorillonite clays). In the latter case up to 10% of the pore water may be adsorbed to the clay (Mitchell, 1993). An increase of volumetric content of adsorbed water leads to a shift of the Atterberg limits (i.e. the liquid limit and plastic limit) towards higher water contents and an increasing swelling and shrinkage potential and therewith to an increase in compressibility and viscosity.

The fabric of clay soils (i.e. the arrangement of the clay particles) is determined by the system of attractive and repulsive forces between the clay particles and the surrounding water. Attractive forces mainly concern Van der Waal's forces, whereas repulsive forces mainly concern the double layer forces. If the net force of interaction at the contact points between the clay particles is attractive, the particles will flocculate, i.e. they tend to move towards each other and become attached. A card house fabric develops, in which the negative surfaces of the clay particles are connected 'edge-to-face' as well as 'face-to-face' by divalent cations (Fig. 2.2(a)). If the net force is repulsive, the particles will disperse, i.e. they tend to move away from each other.

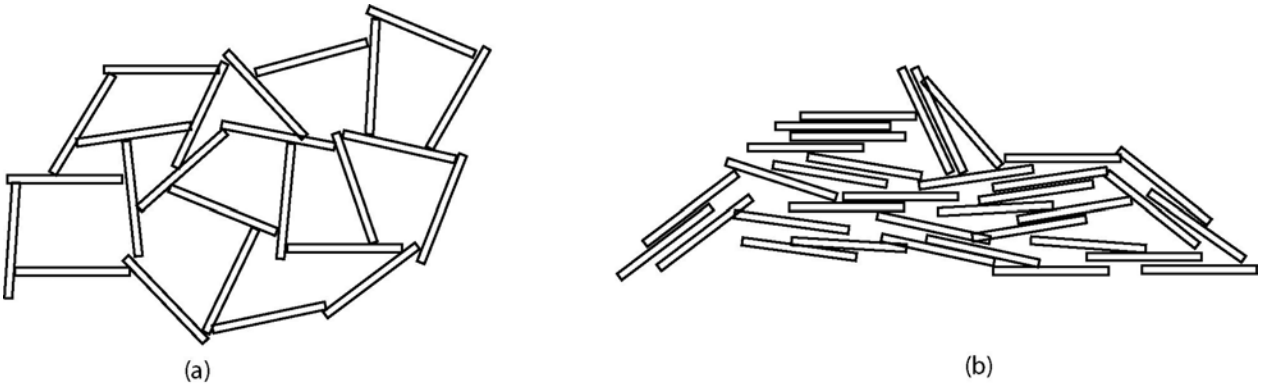

Fig. 2.2. Modes of sedimentation of clay particles: flocculation (a) and dispersion (b) (after Collins and McGown, 1974).

A fabric develops in such a way that the number of contact points is as small as possible. Consequently they tend to align parallel to each other (Fig. 2.2(b)).
The magnitude of the repulsive forces is strongly determined by the thickness of the double layer. Dispersion is enhanced with an increase of thickness of the double layer.

It is obvious that the fabric and (therewith) the mechanical properties of clays strongly depend on the size and valence of the exchangeable cations and the electrolyte concentration of the pore water. Alteration of these factors will consequently result in changes of these properties (see e.g. Xiang, 1997). For example, the high salt content in clays that were deposited in a marine environment, have caused flocculation of the clay (Fig.2.2a). When the clay is removed from its seawater environment the salt will be removed due to leaching by freshwater, resulting in an increase of the thickness of the double layer and therewith a deflocculation (i.e. dispersion) of the clay. A similar process of deflocculation occurs if a clay was deposited in an acid environment (pH<7) and pH increases over 7.

The fabric of clay particles has important consequences for the behaviour of clay under compression and shear stress. Compression and shear stress between the solid particles of the soil are transmitted via contact areas (Persson, 1995). In cohesive soils the nature of these contact areas and stress transmission is complicated. Whereas in cohesionless soils, which have no viscous properties, the grain skeleton does not deform if acting stresses are kept constant, in cohesive soils the contact areas are viscous so that under a constant stress the contact area will deform gradually. For a cohesionless soil applies that only when it undergoes additional compressive stresses the load capacity of the contact areas will be exceeded. This leads to a rearrangement and densification of the grain skeleton in order to increase the number of contact areas, until the loading capacity equals the applied stress. Unloading of the soil mass will then result in some elastic expansion of the grain skeleton, although the new contact areas will be maintained. (The latter means that during reloading the soil material will behave more stiffly). In cohesive soils, however, densification, and therewith the increase of contact areas, also occurs under constant stresses due to volumetric viscous deformation. Consequently the viscous deformation rate decreases over time. If the soil is sheared with a constant stress, but without a

change of volume (i.e. the soil is in critical state), the total of contact areas does not change and deformation rate is constant as well.

Chapter 3 Simulation of large-size creeping natural slopes

3.1 Introduction

Simulation of creep movements in cohesive slopes requires a constitutive relation that describes the overall stress-strain behaviour of soils in an accurate way. As mentioned in the previous chapter, the overall behaviour of the soil is determined by its micromechanical properties. Therefore, if one would know all about the granulometry of the individual particles and understand all the physics and mechanics of the interparticle contacts, it should in principle be possible to predict the overall, macroscopic behaviour of the particles assembly. This would enable the design of a macroscopic constitutive model in which the average macroscopic constitutive parameters could be correlated to the microscopic entities (e.g. correlate the overall critical friction angle to the particle-to-particle friction angle). However, from the previous chapter it has become clear that the micromechanical properties of cohesive soils are very complex and the nature of contact areas and stress transmission between the clay particles remain for a great measure still unknown. Both analytical and numerical models have been developed that try to explain the overall behaviour by microscopical interactions (e.g. Cundall and Strack, 1979, Borja and Wren, 1996). Because of the strong oversimplifications, however, their results were unsatisfactory so that they have had little impact on the current used constitutive models. Moreover, for analysing large-size geotechnical problems, such as the case study presented in Part 2 of this thesis, the description of contacts between individual particles would require huge computer capacities.

However, although very complex when examined on microscopic scale, it appears that soils may be idealized at the macroscale as behaving like continua. At this scale the various properties associated with the individual soil particles are integrated and averaged to the level of a homogeneous continuum. Therefore concepts from continuum mechanics are used to describe the soil's behaviour. Due to the phenomenological approach it is possible to describe the mechanical behaviour of many soils in a proper way, although they may have different micromechanical properties.

A wide variety of constitutive relations for soils has been used for slope stability analysis in literature, varying from very simple linear elastic laws to elastoplastic and elastoviscoplastic laws. Classical elastoplastic laws are based on the classical isotropic plasticity theory (described in e.g. Hill, 1998). Only the elastoviscoplastic material models (which belong to the rheological models and are mostly based on Newton, Bingham or Norton laws) may be suitable for simulation of creeping slopes as they account for viscosity of the soil material. However, many elastoviscoplastic laws are highly complicated (including complex mathematical descriptions of yield surfaces, flow rules and hardening laws) and often not obeying physical laws or experimental observations (e.g. the strict division of deformation in elastic and plastic parts), with the consequence that determination of material parameters and calibration of the model cannot be performed with standard laboratory tests on soil samples. An overview of these models can be found in e.g. Duncan (1996) and Prevost and Popescu (1996).

In recent times hypoplastic and visco-hypoplastic material models are used more and more as an alternative for the elastoplastic and elastoviscoplastic laws respectively. In case of the visco-hypoplastic material model, used in this study, important experimental observations such as creep, relaxation and rate-dependence are described in a more realistic way (e.g. Niemunis, 2003 and Gudehus, 2003). Another important advantage, compared to many of the above-mentioned constitutive laws, is that material parameters can all be determined with standard laboratory tests and are strictly separated from state variables (stress and density). The material law has been validated for many different geotechnical problems (e.g. calculation of slope deformations due to open pit mining (Karcher, 2003)).

In the following the basic principles and equations of visco-hypoplasticity are given.

3.2 Visco-hypoplastic law

The visco-hypoplastic law represents a tensorial, incremental non-linear function, describing the stress-strain-time behaviour of soft soils, i.e. soils consisting of particles having viscous properties. The incremental stiffness, by which strain rate is related to stress rate, depends on density, effective mean pressure and most recent deformation history. The material law was developed as an extension of hypoplasticity, which describes the behaviour of cohesionless granular soils and which distinguishes itself from elastoplasticity by the lack of a yield surface and flow rule. The fundamentals of hypoplasticity can be found in Herle (1997). Modification to visco-hypoplasticity includes the adoption of the critical state concept from the Modified Cam Clay material model which was described by Schofield and Wroth (1968) and Roscoe and Burland (1968). Furthermore, viscous characteristics of cohesive soils are taken into consideration so that creep, relaxation and rate-dependence can be described. The non-viscous part of the law was taken from hypoplasticity. The material law is built up from material parameters on the one hand and state variables stress state and density on the other hand, which are strictly separated.

For the sake of simplicity, in the following the visco-hypoplastic material law is given in non-tensorial form. First the behaviour of cohesive soil is described for drained oedometric compression and creep (Fig. 3.1(a)), then for undrained isotropic compression and finally for non-isotropic compression (e.g. shear, Fig. 3.1(b)), in which critical states can be reached. Presented is the version of Niemunis (2003), with which the simulations in the case study were conducted. An alternative version, which differs in some aspects from the version of Niemunis, can be found in Gudehus (2003).

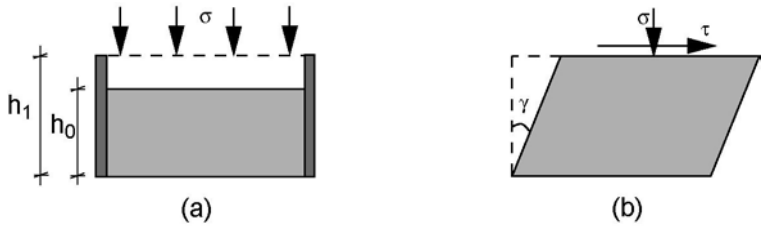

Fig. 3.1. Acting stresses in a oedometer test (a) and shear box test (b). Axial strain is defined by the relation: $\varepsilon = (h_1 - h_0)/h_0$.

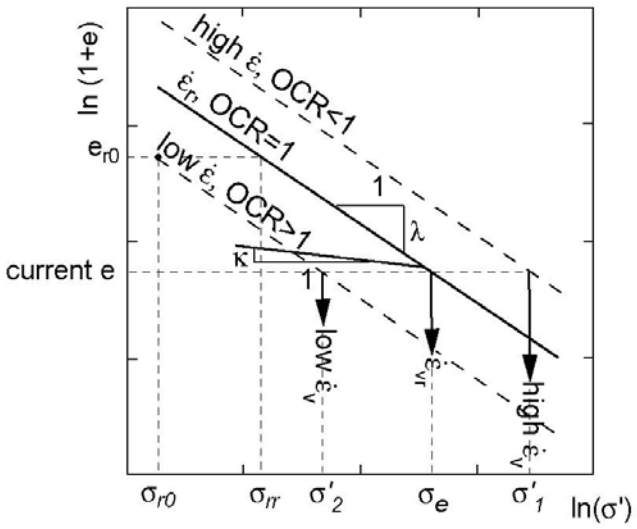

Fig. 3.2. Evolution of void ratio with effective stress for cohesive soil material, if virginally compressed in an oedometer test. The three parallel running straight lines represent isotachs as well as isochrones (see text). $\dot{\varepsilon}$ and $\dot{\varepsilon}_r$ are strain rate and referential strain rate respectively, whereas $\dot{\varepsilon}_v$ and $\dot{\varepsilon}_{vr}$ are creep rate and referential creep rate respectively.

The straight lines in Fig. 3.2 represent the relation between void ratio *e* and axial effective stress σ' due to virgin oedometric compression of a cohesive soil with a constant strain rate $\dot{\varepsilon}$. During compression no excess pore water pressures are allowed to develop. Then the relation between current void ratio *e* and current effective stress σ' (in Fig. 3.2 σ'_1 or σ'_2) after Butterfield is:

$$\ln\left(\frac{1+e_{r0}}{1+e}\right) = \lambda \ln\left(\frac{\sigma'}{\sigma_{r0}}\right) \qquad \text{(Eq. 3.1)}$$

and for unloading/reloading:

$$\ln\left(\frac{1+e_{r0}}{1+e}\right) = \kappa \ln\left(\frac{\sigma'}{\sigma_{r0}}\right) \qquad \text{(Eq. 3.2)}$$

where λ and κ are the virgin compression index and swelling index respectively. e_{r0} is referential void ratio and σ_{r0} referential stress, which is described by the relation:

$$\sigma_{r0} = \sigma_{rr}\left[1 + I_v \ln\left(\frac{|\dot{\varepsilon}|}{|\dot{\varepsilon}_r|}\right)\right] \approx \sigma_{rr}\left(\frac{|\dot{\varepsilon}|}{|\dot{\varepsilon}_r|}\right)^{I_v} \qquad \text{(Eq. 3.3)}$$

where I_v is the viscosity index after Leinenkugel (1976), σ_{rr} is referential stress and $\dot{\varepsilon}_r$ referential strain rate.

The Overconsolidation Ratio (OCR) is defined by the relation:

$$\mathrm{OCR} = \frac{\sigma_e}{\sigma'} \qquad \text{(Eq. 3.4)}$$

where σ_e is the equivalent stress after Hvorslev. This is the stress required to obtain void ratio *e* if a soil sample is virginally compressed in an oedometer test with a referential strain rate $\dot{\varepsilon}_r$ and is described by the relation:

$$\sigma_e = \sigma_{r0}\left(\frac{1+e}{1+e_{r0}}\right)^{1/\lambda} \qquad \text{(Eq. 3.5)}$$

If $\dot{\varepsilon} = \dot{\varepsilon}_r$, all *e*-ln$\sigma$ states lie on the referential isotach for which OCR=1 (Fig. 3.2).

Otherwise,

$$\mathrm{OCR} \approx \left(\frac{\dot{\varepsilon}_r}{\dot{\varepsilon}}\right)^{I_v} \qquad \text{(Eq. 3.6)}$$

holds (Gudehus, 2003).

The above described behaviour of rate-dependence (also called argotropy) can be described with a single constitutive relation:

$$\dot{\sigma}' = -\frac{\sigma'}{\kappa}\left(\dot{\varepsilon} - \dot{\varepsilon}_v\right) \qquad \text{(Eq. 3.7)}$$

Eq. 3.7 is the basic one-dimensional visco-hypoplastic equation and states that the effective stress rate $\dot{\sigma}'$ is a function of the elastic strain rate $\dot{\varepsilon}_{el} = \dot{\varepsilon} - \dot{\varepsilon}_v$ and an incremental stress-dependent stiffness $\frac{\sigma'}{\kappa}$.

$\dot{\varepsilon}_v$ is the viscous strain rate or creep rate (see Fig. 3.2) and described by Norton's power law (Norton, 1929):

$$\dot{\varepsilon}_v = -\dot{\varepsilon}_r\left(\frac{\sigma'}{\sigma_e}\right)^{1/I_v} = -\dot{\varepsilon}_r\left(\frac{1}{\mathrm{OCR}}\right)^{1/I_v} \qquad \text{(Eq. 3.8)}$$

The three parallel running straight lines in Fig 3.2 are isotachs as well as isochrones. With isotach is the line on which all points lie that belong to the same strain rate meant. An increase of strain rate leads to a higher position of the isotach.

With isochrone is the line on which all points lie that belong to the same time of creep (viscous strain) meant. Creep leads to a reduction of the void ratio, an increase of OCR and therewith a shift to a lower positioned isochrone.
For all points lying on the same isotach/isochrone creep rate $\dot{\varepsilon}_v$ is the same. This means that the creep rate of a soil is independent of the path along which it has reached its actual state.

During undrained shearing, or anisotropic compression, the initial ductile behaviour of the soil eventually leads to a critical state. In the following it is shown in which way visco-hypoplasticity describes this process. First the soil behaviour under undrained isotropic compression is discussed. Then the behaviour under anisotropic conditions is described, on which basis the critical state behaviour can be explained. Both isotropic, anisotropic and shear conditions can be described considering an undrained triaxial test (on saturated material, so the volume remains constant), as shown in Fig. 3.3.

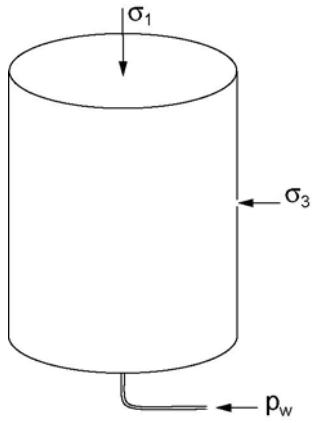

Fig. 3.3. Stresses acting in a CU-triaxial test. p_w is pore water pressure, required for calculation of effective stress: $\sigma' = \sigma - p_w$.

p' is effective mean pressure and defined with $p' = (\sigma_1' + 2\sigma_3')/3$. q is deviatoric pressure and defined with $q = \sigma_1 - \sigma_3$.

Analogous to Eq. 3.2 (oedometric compression) isotropic compression is defined by the relation:

$$\ln\left(\frac{1+e_{r0}}{1+e}\right) = \lambda \ln\left(\frac{p_e}{p_{r0}}\right) \qquad \text{(Eq. 3.9)}$$

in which p_e is the equivalent pressure after Hvorslev and defined analogous to Eq. 3.5. e_{r0} and p_{r0} are referential void ratio and mean pressure respectively if the soil is compressed with a strain rate $\dot{\varepsilon}_r$ (Fig. 3.4(a)). All *p*-*e* states lie on the referential isotach for which OCR=1.

For the description of non-isotropic stress states (so in the case that also deviatoric stresses are accounted for, i.e. $q \neq 0$) the yield function of the Modified Cam Clay material model of Schofield and Wroth (1968) and Roscoe and Burland (1968)) is used. This function describes in the *p*-*q*-graph a so-called yield surface, which has a half-ellipse shape, as shown in Fig. 3.4(c).

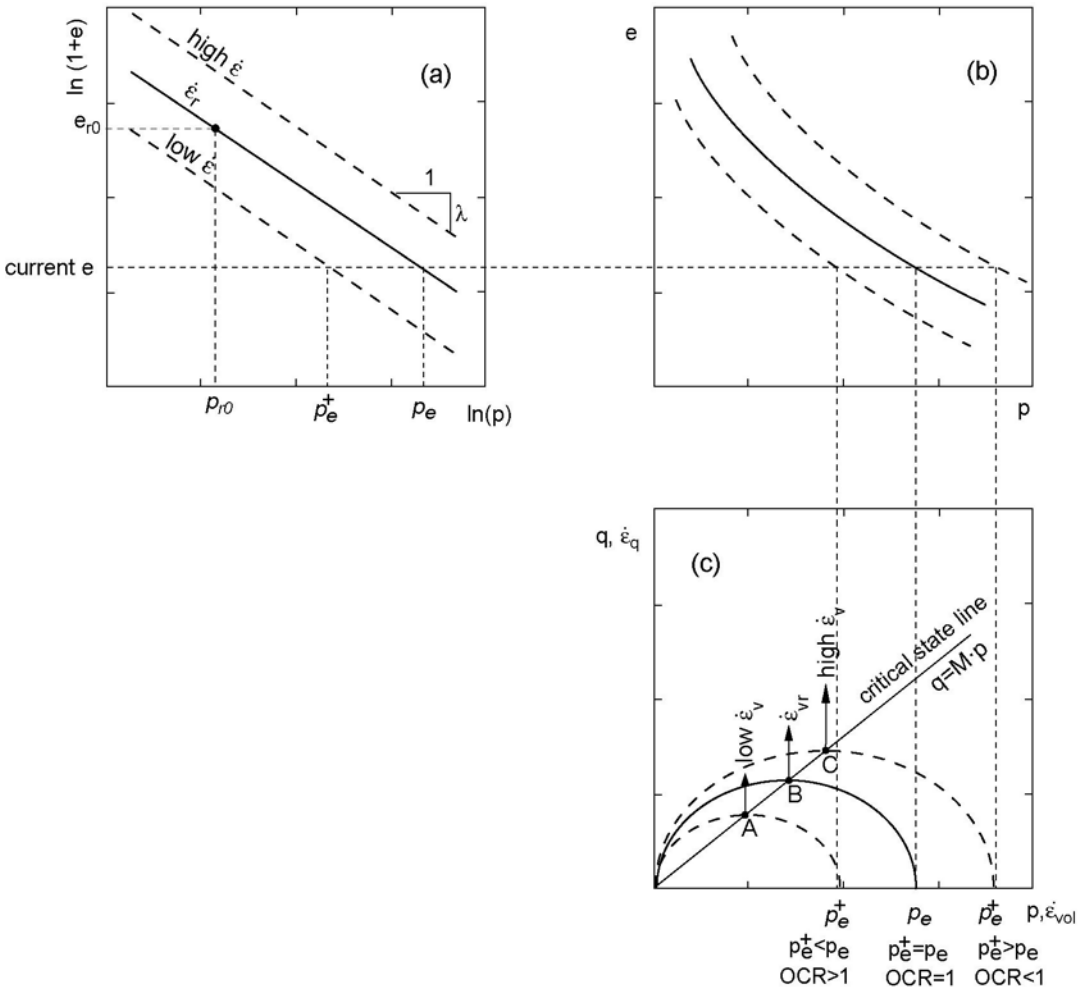

Fig. 3.4. Undrained shearing paths (c) for three different strain rates $\dot{\varepsilon}$ (a referential strain rate $\dot{\varepsilon}_r$ as well as a higher and a lower one), reaching different ultimate stresses (points A, B and C), although they have the same void ratio *e*. The isotachs in (a) and (b) refer to isotropic states (so in (c) points in which $q=0$). Each of the yield surfaces (the half-ellipses in (c)) represents an $\mathrm{OCR} = p_e / p_e^+$ =constant. Creep in A, B and C is purely deviatoric, $\dot{\varepsilon}_{vr}$ is the referential creep rate.

The shape of the yield surfaces is constant, but the dimensions are variable in dependence of void ratio and strain rate (Fig. 3.4(a-c)). Yield surfaces having a smaller dimension than the referential half-ellipse, refer to overconsolidated states (OCR>1). On each point on the yield surface the creep rate $\dot{\varepsilon}_v$ is the same. Points in the *p*-*q*-graph in which *q*=0 represent isotropic stress states.

The Overconsolidation Ratio OCR is defined by the relation:

$$OCR = \frac{p_e}{p_e^+} \qquad \text{(Eq. 3.10)}$$

where p_e^+ is the pressure for a particular state under isotropic conditions (determined by the yield surface, see Fig. 3.4(c)) and is described by the relation:

$$p_e^+ = \frac{p}{\beta - 1}\left[\beta\sqrt{1+\eta^2\left(\beta^2-1\right)}-1\right] \text{ for } \eta < 1 \qquad \text{(Eq. 3.11)}$$

and

$$p_e^+ = p(1+\eta)\frac{1+\beta}{2} \text{ for } \eta > 1 \qquad \text{(Eq. 3.12)}$$

where β ($0 < \beta < 1$) is a material parameter that defines the shape of the yield surface (for determination is referred to Niemunis (2003)) and $\eta = \frac{q}{Mp}$. M will be defined below (Eq. 3.13).

Only for the case that either strain rate or stress rate is constant, OCR is constant as well. If no deformation takes place, OCR will increase due to stress relaxation. If stresses are fixed, OCR will increase due to volumetric creep.

The direction of (viscous) strain is for all stress states perpendicular to the yield surface (Fig. 3.4(c)).

The soil reaches its critical state when its *p*-*q* state lies on the so-called critical state line (CSL) (in Fig. 3.4(c) points A, B and C). The slope of the CSL is defined by M:

$$M = \frac{q_c}{p'} = \frac{6\sin\varphi_c}{3-\sin\varphi_c} \qquad \text{(Eq. 3.13)}\ [1]$$

[1] In the version of Niemunis (2003), *M* also depends on a pressure-dependent factor, obtained from the Matsuoka-Nakai-criterion. For the sake of simplicity this has been left out in this equation.

where φ_c is the critical friction angle, which is a material constant, and q_c is the critical deviator stress from which the maximum shear strength c_u can be obtained by the relation:

$$c_u = \frac{q_c}{2} \qquad \text{(Eq. 3.14)}$$

When the soil is in a critical state, only shear without change of volume occurs and creep is purely deviatoric.

For the visco-hypoplastic equations in tensorial form is referred to Niemunis (2003). By writing the equations for the three-dimensional case in tensorial form, independence of the coordinate system is provided and also the direction of (viscous) strain can be described. This is required for implementation of the material model into the FE-method.

3.3 Visco-hypoplastic material parameters

Table 3.1 shows the visco-hypoplastic material parameters, which all can be determined by means of standard laboratory tests. The parameters κ and λ are determined by means of oedometer tests as shown in Fig. 3.2.

Tab. 3.1. Description of the visco-hypoplastic material parameters and methods for their determination.

Symbol	Unit	Description	Method for determination
e_{100}	[-]	Void ratio during isotropic compression with referential strain rate $\dot{\varepsilon}_r$ at 100 kPa	Oedometer test
$\dot{\varepsilon}_r$	[s^{-1}]	Referential strain rate	
λ	[-]	Compression index	Oedometer test
κ	[-]	Swelling index	Oedometer test
φ_c	[°]	Critical friction angle	Triaxial test
I_v	[-]	Viscosity index	Triaxial or oedometer test

The parameter e_{100} is the void ratio during isotropic compression with referential strain rate $\dot{\varepsilon}_r$ at 100 kPa and represents the e_{r0}-σ_{r0} state in Fig. 3.2. Since the visco-hypoplastic parameters λ, κ and e_{100} have to be defined under isotropic conditions, the values determined by means of oedometer tests must be converted. Relations for conversion can be found in Niemunis (2003). Critical friction angle φ_c is determined by means of a CU triaxial test and obtained by Eq. 3.13 and Fig. 3.5(a).

Viscosity index I_v can be determined by means of a CU triaxial test with a velocity jump (i.e. $\dot{\varepsilon}_r$ is increased to $\dot{\varepsilon}$, as shown in Fig. 3.5(b)), and defined by the relation:

$$I_v = \frac{\ln\left(\frac{q}{q_r}\right)}{\ln\left(\frac{\dot{\varepsilon}}{\dot{\varepsilon}_r}\right)} \qquad \text{(Eq. 3.15)}$$

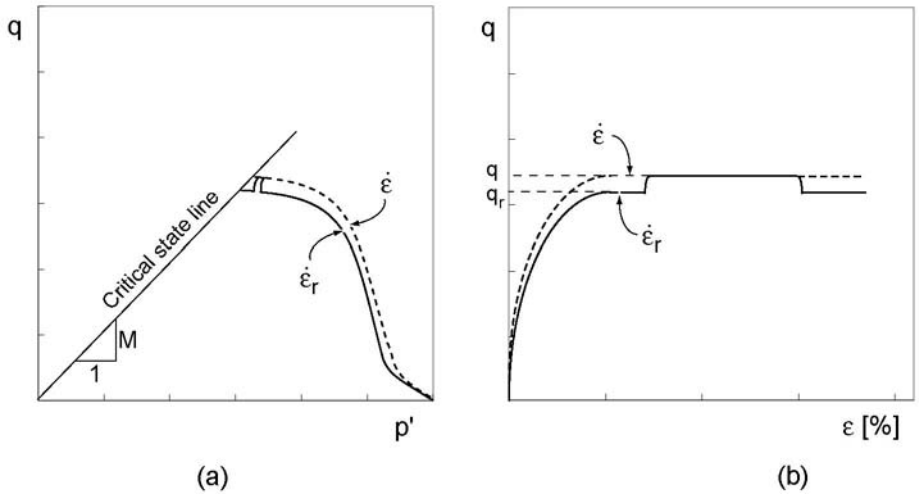

Fig. 3.5. Stress path (a) and stress-strain curve (b) for a CU triaxial test with velocity jump from $\dot{\varepsilon}_r$ to $\dot{\varepsilon}$ and $\dot{\varepsilon}_r > \dot{\varepsilon}$, in order to determine φ_c (with Eq. 3.11) and I_v.

Alternatively I_v can also be determined by means of an oedometer test (see Niemunis, 2003) or estimated with the empirical relation (Krieg, 2000):

$$I_v \approx 0{,}05 + 0{,}026 \ln w_L \qquad \text{(Eq. 3.16)}$$

in which w_L is the liquid limit.

3.4 Spatial variation of material properties and state variables

Although the overall behaviour of soils can be described by considering the soil as a continuum, the description of some phenomena can only be explained and simulated by considering heterogeneities on the particle level. The most important one is strain localisation, i.e. the process by which the deformations in a soil tend to localise into narrow bands of intense straining. This phenomenon often leads to catastrophic failure of the slope as the shear bands may develop into continuous slip planes. The initiation of localisation seems to be related to microscopic heterogeneities in the soil fabric, due to different grain sizes, heterogeneities in particle arrangements and differences in the mechanical behaviour of the individual soil particles, leading to variations in state variables like stress and density (Yoshida et al., 1974).

Nübel and Karcher (1998) were able to simulate strain localisation patterns in a granular (cohesionless) soil realistically with the FE-method and using a hypoplastic material law. The initial void ratio, assigned to the FE-mesh, was varied spatially between the highest and lowest values that are physically possible, according to a frequency distribution. The use of a polar continuum (a so-called Cosserat continuum, in which the material points have an additional degree of freedom for rotation) provided localisation to be mesh-independent.

In granular materials the thickness of the shear bands appears to be approximately 5 to 10 times the grain size (Nübel, 2002). For FE-simulation this means that the element size must be smaller than the thickness of the shear band. Also a realistic representation of microscopic void ratio distribution would require a very small element size. Therefore, in case of a large-sized problem such as the case study presented in this thesis, realistic incorporation of shear localisation into the model would not be possible due to high costs, both in time and computer capacity.

In the visco-hypoplastic law, as presented in the previous section, strain localisation has not been incorporated yet and will therefore not be accounted for in the case study in Part 2. (In chapter 5 it will be shown that this is no shortcoming, as inclinometer measurements did not reveal the presence of significant shear zones). According to Gudehus (2003) the gradient of excess pore water pressure (in case of a low initial OCR) or gradient of suction (in case of a high initial OCR) control the development of localisation.

For simulation of slope movements, it is necessary to design a subsurface model that is subdivided into zones of homogeneous properties. However, a large-sized geotechnical problem, such as presented in this thesis, often shows a very complex and heterogeneous material distribution, due to facial changes during sedimentation (which may for example result in a rapid alternation of cohesive clay layers and cohesionless sandy layers) or due to more recent slope processes (for example mixing of materials within an earth flow). Borehole records often provide such very fine-scaled information. However, besides the fact this information solely refers to a discrete point in space, it can often not be incorporated in the model or only with large efforts (e.g. the construction of a very complex FE-mesh). Therefore the complex subsurface model, consisting of a large number of small layers, has to be simplified into a model built up from a smaller number of larger homogeneous zones. This, however, is only allowed if the (time-dependent) stress-strain behaviour of the homogenised model is equal to that of the original subsurface model (as far as it is possible to verify this).

Fig. 3.6 shows two methods of homogenisation for a soil consisting of sequence of several clay and sand layers. A first method involves the joining of both sequences of layers into two homogeneous units, in which the total volume fractions of both materials are kept unchanged (Fig. 3.6(a)).

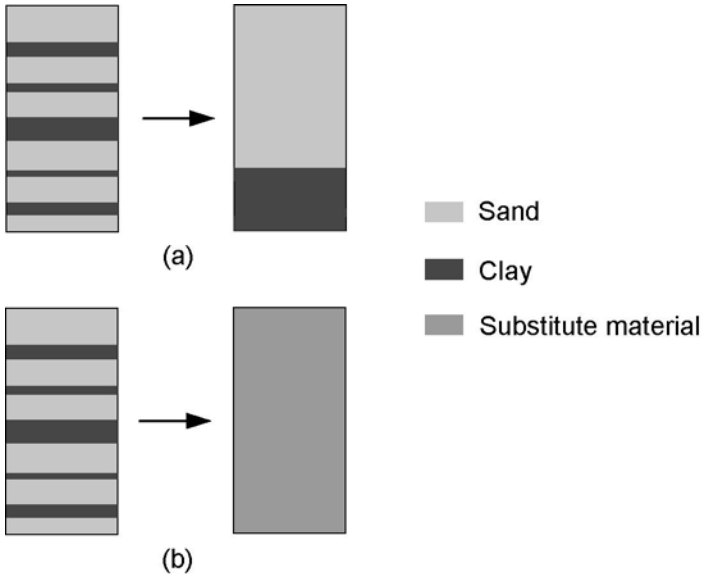

Fig. 3.6. Homogenisation of a sequence of clay and sand layers by means of joining (in which the volume fractions are not changed) (a) or by means of conversion into a substitute material (b).

Alternatively, the complete sequence of sand and clay layers can be replaced by a single substitute material, subject to the assumption that any mixture of these materials would lead to a proportional mixture of the material's properties (Fig. 3.6(b)).

Karcher (2003) proved the validity of the first method (Fig. 3.6(a)) by comparing the stress-strain behaviour of different material arrangements of two different materials by means of FE-simulation (Fig. 3.7), using a hypoplastic material law and using the same boundary and initial conditions for every arrangement. The results appeared to be very similar for both shearing and compression. It could therefore be concluded that homogenisation of layers according to this method is allowed if deformation occurs by means of shearing and/or compression. This makes the method suitable for simulation of slope deformations.

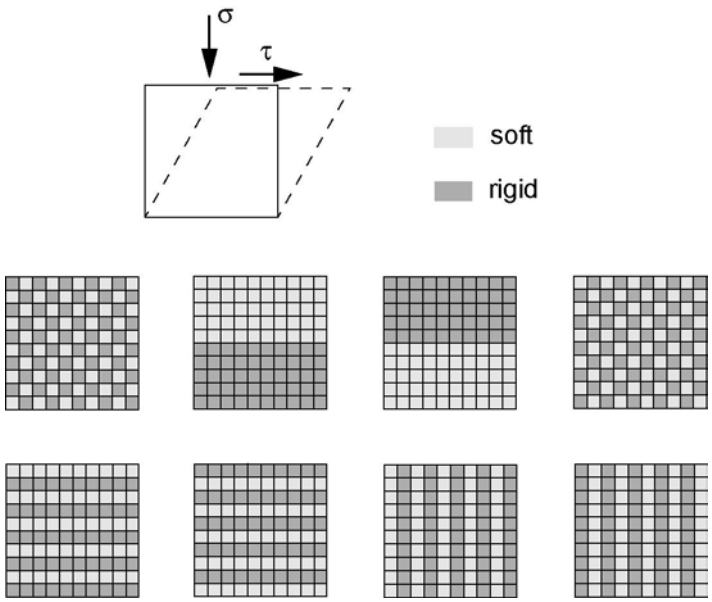

Fig. 3.7. Different material arrangements in a FE-mesh of 10x10 m in order to investigate the influence of homogenisation on the stress-strain behaviour (after Karcher, 2003).

For both methods it should be noted that homogenisation is not allowed if one of the layers to be homogenised has a decisive influence on the overall behaviour, e.g. in case of a very weak clay layer that acts as a lubricant.

3.5 Methods for generation of an initial stress state

The visco-hypoplastic law consists of material parameters, which are constants, and the state variables density and stress. Stress and density (which, together with deformation rate, determine OCR) strongly affect the viscous behaviour of the soil. Therefore a realistic initial stress state and density distribution have to be assigned to the model with which the slope deformations have to be simulated. This can be done on the basis of measurements or by means of simulation or estimation.

As has become clear in section 3.2, the density distribution within a slope is determined by the presently acting stresses as well as the slope history. After its deposition the material is densified continuously due to volumetric creep accompanying shear creep. This means that for obtaining realistic initial state variables by means of simulation, slope history should in principle be simulated completely. In many cases, however, too little information is available (e.g. in case of slope conditions that change over time), which makes this method inapplicable. If information of the void ratio distribution of the slope is available (e.g. from water contents measured on materials from the borehole logging in different depths), the simulated void ratio distribution may be compared to the measured one in order to verify the accuracy of the simulated initial state.

The ratio between horizontal and vertical stresses (expressed by the coefficient of earth pressure at rest, K_0) is often estimated by the equation of Jaky:

$$K_0 = \frac{\sigma_h}{\sigma'_v} = 1 - \sin\varphi_c \qquad \text{(Eq. 3.17)}$$

For overconsolidated cohesive soils, Kolymbas (1998) relates K_0 to OCR by the relation:

$$K_0 = \frac{\sigma_h}{\sigma'_v} = \left(1 - \sin\varphi_c\right) \cdot \mathrm{OCR}^{\alpha} \qquad \text{(Eq. 3.18)}$$

with $\alpha \approx 0{,}5$.

The reason for the lower horizontal stresses compared to the vertical ones within the slope are shear stresses. In cohesive soils, however, shear stresses may relax over time due to viscosity, resulting in an increase of K_0 (in theory eventually a hydrostatic stress state (i.e. $K_0 = 1$) is reached if relaxation time is long enough).

3.6 Finite Element Method

A part of the simulations presented in Part 2 were performed using the Finite Element (FE) programme Abaqus (Abaqus Version 6.5-1), in which the visco-hypoplastic law was implemented. In the following some basic principles of the FE-method are given.

The FE-method is a numerical technique for solving boundary value problems approximately (Bathe, 1990), in which the solution space is discretised into a number of finite elements. As the visco-hypoplastic equations are non-linear, the boundary value problem has to be solved by means of an incremental-iterative approach, which can be explained as follows: external forces, or prescribed displacements, are applied in a number of increments. In each increment an equilibrium has to be found by means of iterations, until the (predefined) convergence criterion has been fulfilled, i.e. the force residual (i.e. the difference between external and internal forces) is less than the current tolerance value (the latter has to be prescribed). For doing this Abaqus uses the Newton-Raphson iteration scheme (Abaqus Inc., 2004).

Detailed information about the FE-analysis can be found in e.g. Bathe (1990). For implementation of the visco-hypoplastic law in the FE-method is referred to Niemunis (2003).

Concerning the temporal and spatial discretisation of the boundary value problem, it should be noticed that it must always be verified that the calculated deformations are independent of the size of the time increment at the one hand and the size, type (in Abaqus several types of elements are available, which differ in shape, order (i.e. number of nodes) and level of integration (i.e. number of integration points)) and arrangement of the elements on the other hand.

Part 2 Case study

Chapter 4 Introduction to the case study

4.1 Introduction

In Part 1 of this thesis the basic principles of the mechanical behaviour of cohesive soils, approached on a microscopic level, and the description of this behaviour by the visco-hypoplastic law were discussed. Furthermore, some methods for dealing with the limited availability of subsurface data with respect to the design of a proper subsurface model were discussed.
The objective of Part 2 is to test the applicability of the visco-hypoplastic law for predicting the creep movements of a large-size natural slope by means of numerical simulation. Besides on the validity of the constitutive law, the model performance strongly depends on the accuracy of incorporation of the initial state variables, material parameters and distribution, pore water pressure distribution and slope geometry into the model. However, due to the limited availability of subsurface data, simplifications and assumptions concerning the above mentioned factors had to be made. A second objective of this part, therefore, is to quantify the uncertainty of the model due to these simplifications and assumptions by means of sensitivity analyses.

This chapter discusses the general methodology applied and gives an introduction to geography and geology of the study area.
Chapter 5 describes the slope history and gives a detailed material characterisation as well as the results of geotechnical in-situ measurements that were carried out at the slope. The two numerical models that were used, were designed based on these data and the simulation results were compared with measurements of the slope movements.
Chapter 6 finally deals with the simulation of the creep movements, including a detailed description of the methods used for designation of the two models, determination of material parameters and initial state variables. Finally the results of the simulations and a number of sensitivity analyses are discussed.

4.2 Approach

Simulation of slope movements with the visco-hypoplastic law requires, besides the definition of the material parameters and initial stress state, a numerical programme that is capable to solve the posed boundary value problem. In this study two different types of numerical models were applied: a relatively simple element test programme and the FE-programme Abaqus (Abaqus Inc., 2004). With the element test programme (which was originally developed for simulation of laboratory element tests, such as oedometer and triaxial tests) small slope sections were simulated, which were considered to be a single element. Since within the element material properties and distribution of state variables are homogeneous, the size of the element has to be kept be rather small. Furthermore, a complex slope geometry cannot be incorporated into the model. The FE-method does not suffer these limitations. Dependent on the resolution of spatial discretisation, heterogeneity in material distribution can be incorporated and state variables can vary spatially within the FE-mesh. Therefore this method allows simulation of larger slope sections as well as analysis of spatial distribution of displacements and velocities.

In order to compare both models which each other and to evaluate to what extent the simplifications of the element test model compared to the FE-model affect the model performance, simulations were performed using the same set of material parameters, initial state variables and boundary conditions.

A study slope was selected on which the models could be tested. Because of the availability of an extended data set with high resolution, both in spatial and temporal view (which can be considered to be quite unique for a slow moving natural slope), the Stambach slope in Upper-Austria was chosen. This is an inactive earth flow that was activated in 1982 for the last time. Since that time the slope is in a creep stadium. A great part of the data used in this study originate from the work of Rohn (1991). Xiang (1997), who investigated the relation between the mechanical and rheological behaviour of the slope materials and the characteristics of the clay minerals, and Fernandez-Steeger (2002), who predicted mass movements by means of neural networks, used the Stambach slope as a case study.

The available data were prepared and, if necessary, completed. From borehole records and seismic measurements the slope geometry was determined on which' basis a two-dimensional subsurface model was designed. Based on geological knowledge and geotechnical mapping the material distribution was assessed. This way representative soil samples could be taken, on which the visco-hypoplastic material parameters were determined by means of laboratory element tests (oedometer and triaxial tests).

The visco-hypoplastic law was validated for these materials by simulating the oedometer and triaxial tests, using the obtained material parameters (with validation is meant testing whether the visco-hypoplastic law is able to reproduce the experimental results). This was done using an element test programme in which the visco-hypoplastic law was implemented.

Using the element test programme and FE-method the slope movements were simulated. The methods used for both the element test simulations and FE-simulations (especially determination of the initial state variables and establishment of the boundary conditions) are described in detail in sections 6.4 and 6.5 respectively. The simulation results were compared with available inclinometer measurements.

Finally, for both models a sensitivity analysis was performed in order to quantify the influence of simplifications and assumptions concerning the initial state variables, boundary conditions, material distribution and slope geometry. This way the uncertainty of the model performance due to the limited availability of subsurface information at the one hand and the limited possibility to incorporate the available information in the model at the other hand could be quantified.

4.3 Description of the study area

4.3.1 Geographical setting

The study slope (Fig. 4.1) is located in the province of Upper-Austria (Austria), above the village of Bad Goisern in the Traun Valley (see Fig. 4.2), around 50 km southeast of Salzburg. The slope

studied is part of the Stambach catchment, which covers an area of around 8,5 km^2 and discharges into the Traun River.

Fig. 4.1. View on the slope from the south, directly after the last activation of the earth flow in 1982 (Austrian Service for Torrent and Avalanche Control in Bad Ischl).

The catchment stretches from 525 m.a.s.l. at the Traun River to a height of 1326 m.a.s.l. at the Zwerchwand. The latter is an around 80 m high, steep rock face, upslope and adjacent to the study slope.

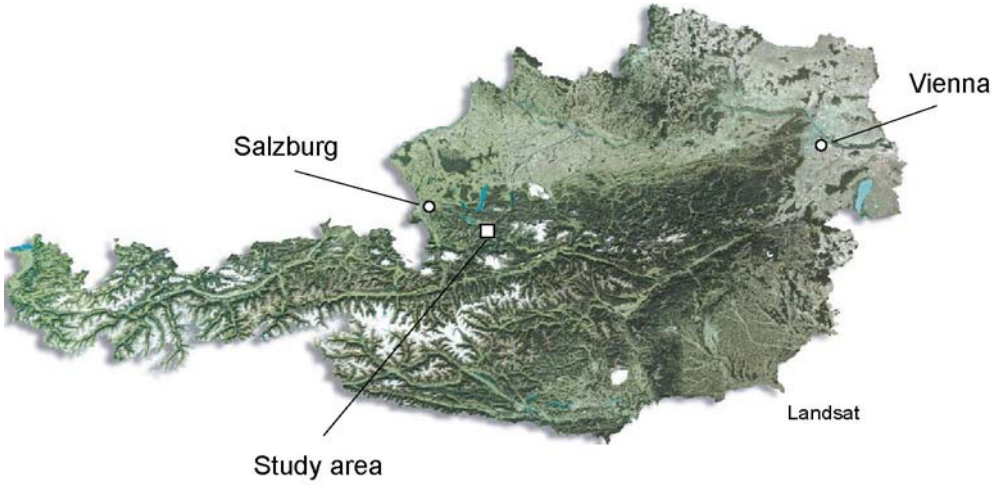

Fig. 4.2. Location of the study area (Landsat satellite image).

4.3.2 Geology

The study area belongs to the middle part of the Eastalpine part of the Northern Calcareous Alps (NCA), and is built up mainly from Permian to Jurassic sediments. Geographically, the middle part of the NCA is a 40-50 km wide, West-East running zone that stretches from the Rhine Valley in the west to the Vienna Basin in the east (Plöchinger, 1982).
Palaeographically, the NCA are the northern, distal (adriatic) continental shelf of the Tethys Ocean, which was sheared off due to the Alpine Orogeny. Tectonically the NCA can be subdivided into three main tectonic units. The lowest nappe is the Bajuvaricum. Hereupon follows the Tirolicum, forming the middle and largest part of the NCA. The highest nappe is the Juvavicum. The latter can be subdivided into the Lower Juvavicum of the Hallstatt Facies ('Hallstatt Zone of Bad Ischl-Bad Aussee') and the Upper Juvavicum of the Dachstein Facies (Dachstein Nappe). The study area belongs to the 'Hallstatt Zone of Bad Ischl-Bad Aussee'.

The sequence of sedimentation in the Hallstatt Facies started during the Perm with the deposition of evaporites and siliciclastics in marine basins (Haselgebirge Formation) (Mandl, 2000), which were formed in the Variscan basement due to basin-and-range extension (Eisbacher, 1996).
During the Trias this extension and associated subsidence proceeded and a passive continental shelf edge developed. During the Lower Trias shallow-sea sediments ('Werfen' Formation and 'Gutenstein' Formation) were deposited. Due to proceeding subsidence in the Middle Trias, a differentiation in shallow carbonate platforms and deep basins developed (see Fig. 4.3). In the back-platform lagoon area and the reef area the series belonging to the Hauptdolomite Facies and Dachstein Facies ('Wetterstein' Dolomites) were deposited respectively, while in the deep basins the series belonging to the Hallstatt Facies ('Bunte Hallstatt' and 'Pötschen' Limestone Formations) were deposited (Mandl, 2000).

Due to the increasing terrigenous influence at the end of the Trias, marly and limy series ('Zlambach' Formation and 'Allgäu' Formation) were deposited, a process that continued up to the Dogger. During the Dogger the carbonate platforms started to disintegrate and the Austro-Alpine shelf to subside, while the Palaeotethys was almost completely closed and the Penninic Ocean just started to open. This subsidence resulted in the deposition of siliceous radiolarites.

During the initial phases of the Alpine Orogeny, at the end of the Jura and the begin of the Upper Cretaceous, again a differentiation of the ocean floor took place, resulting in deposition of carbonates on the platforms (‘Tressenstein’ and ‘Oberalm’ Formations) and pelagic limestones in the basins lying in between (‘Oberalm’ Formation) (Mandl, 2000).

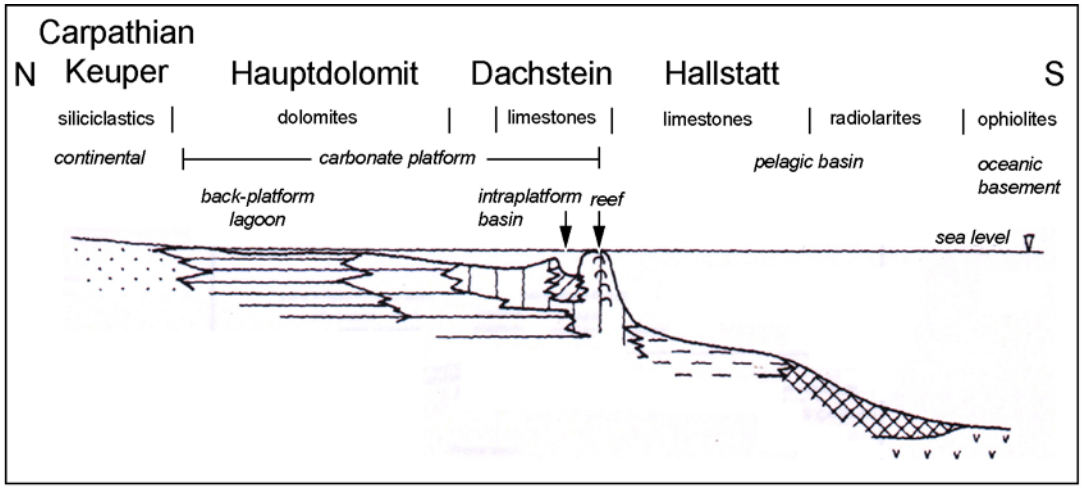

Fig. 4.3. Facies distribution of the continental edge in the NCA (changed after Mandl, 2000).

Due to increasing terrigenous influence and increasing depths of water during the Upper Cretaceous, marly series were deposited (‘Schrambach’ Formation). During the Middle Jura sandy marls (‘Roßfeld’ Formation) were deposited in a syntectonic clastic facies at the front of the developing alpine nappes. In the Middle Jura the marine sedimentation in the Eastern Alps was finished. During the Malm isostatic uplift of the area started. The increasing plate convergence, resulting in a push into a northern direction, led to fragmentation and overthrusting of the marine series.

The position of the Hallstatt Facies (a basin facies) between the Hauptdolomite Facies (a lagoon facies) in the North and the Dachstein Facies (a reef facies) in the South is up to now not completely clarified. According to a first theory (e.g. Medwenitsch, 1957) the Hallstatt Zone was developed north of the Dachstein Nappe. During the Alpine Orogeny the Hallstatt Nappe was partly overthrust by the Dachstein Nappe and was thrust onto the Hauptdolomite Nappe together with the latter one.

Another theory (e.g. Schäffer, 1976 and Mandl, 2000) states that the Hallstatt Zone was developed south of the Dachstein Nappe (see Fig. 4.3). During the Orogeny the Hallstatt Nappe thrust over the entire Dachstein Nappe onto the Hauptdolomite Nappe.

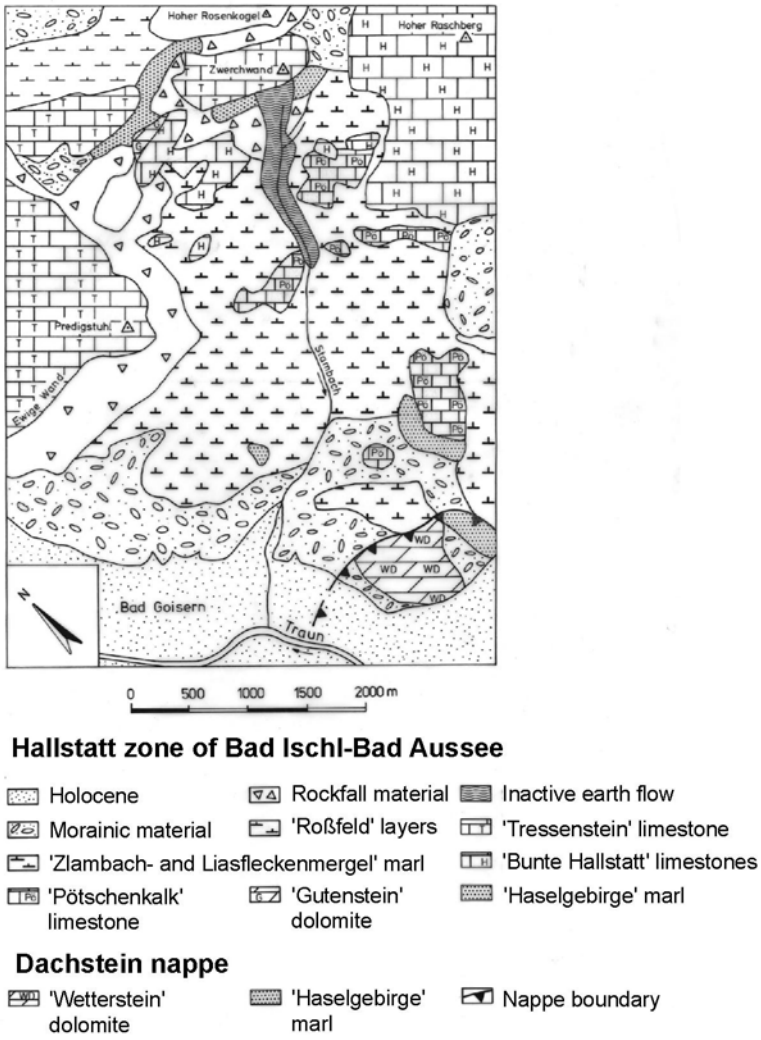

Fig. 4.4. Geological map of the area surrounding the study slope (changed after Schäffer, 1982 and Rohn, 1991).

During the Pleistocene the study area was covered by glaciers for several times. The last major glaciation was the Würm Glacial, in which the ice reached its maximum level of around 1 600 m at the height of the study area for about 22-18 000 year b.p. (Van Husen, 1977). Glacial erosion led to oversteepening of the valley walls. As during deglaciation the up to that moment stabilising counter pressure of the glacier was removed, many mass movements developed. A large number of large-size mass movements in the vicinity of the study area can be correlated to the several

phases of glacial retreat (Van Husen (1977) mentions a total of 5 phases between 17 000 and 11 000 b.p.). It is very likely that also the Stambach earth flow was activated for the first time immediately after deglaciation. This was supported by radiocarbon analysis on organic material, taken from within the slide mass, which could be dated on 9 700±500 yr b.p. (Rohn et al., 2004). In section 5.1 the history of the slope will be described in more detail.

In the following a short description is given of the relevant lithological units in the study area (i.e the source areas of the earth flow). These are Permian-Triassic claystones of the Haselgebirge Formation, Triassic and Jurassic marls of the Zlambach Formation and Allgäu Formation respectively and Jurassic limestones belonging to the Tressenstein Formation, as shown in Fig. 4.4 (other geological maps of the area can be found in e.g. Weigert, 1971). The mineralogical composition and mechanical properties of the materials of the slide mass will be discussed in chapter 5.

Haselgebirge (which literally translated means 'salt rock mass') in undisturbed form is an unstratified mixture of claystone, rock salt and anhydrite, with occasionally some sandstone layers (Schauberger, 1978). Up to depths of 70 m from the surface the salt has been leached out completely and, if present, anhydrite has been converted into gypsum. This form of Haselgebirge predominantly consists of red and grey-green, silty clays, containing blocks of gypsum and fragments of siltstones. Haselgebirge in unweathered form is not encountered in the study area.

The stratigraphical lower part of the Zlambach Formation (with which the Triassic depositions in the Hallstatt Facies were finalised) consists of thin, greyish to brownish, laminated marl layers alternating with limestone layers (Tollmann 1976). Towards the stratigraphical upper parts a transition to shaly marl and claystone layers takes place. The latter are much more vulnerable to weathering.

The Allgäu Formation (of which the marly part is called Liasfleckenmergel Formation) consists of well-stratified grey, marly limestone layers alternating with thin, spotted ('flecken') marl layers. Here and there, especially in the stratigraphical upper parts, siliceous sequences can be found.

Rohn (1991) proposed to use the term 'Fleckenmergel' as a generic name for both the Jurassic marls of the Allgäu Formation and the Triassic marls of the Zlambach Formation, as they can only be distinguished based on micropalaeontological differences (macro-fossils are lacking). In the following chapters solely this term will be used to indicate both materials.

The Tressenstein Formation consists of massive, thickly bedded, light brown or yellowish-white carbonates which have a fine-brecciated character.

The main part of the area surrounding the study slope is built up from Fleckenmergel. Only the upper part of the slide mass, directly below the Zwerchwand, is underlain by Haselgebirge. The massive Tressenstein Limestones, in which the Zwerchwand has been built, lie discordantly upon the Haselgebirge. All formations generally dip to the North.

In the upper part, around the water divide near the Zwerchwand, locally some remnants of morainic material were found. Considering their location of deposition, they are most likely subglacial tills. Subglacial tills are materials of all grain sizes and unbedded. Mostly they are overconsolidated, due to the weight of the former glacier ice.
Into a downhill direction of the study slope larger parts of the Fleckenmergel are covered by morainic deposits (predominantly subglacial tills).

Chapter 5 The Stambach slope

5.1 Slope history

The Stambach slope is a dormant earth flow which was active in 1982 for the last time. According to radiocarbon dating on organic material, taken from within the slide mass, the earth flow was activated at least another three times since the Pleistocene (Rohn et al., 2004): 2 300, 4 500 and 9 700 b.p. (all ±500 yr.). The earth flow almost completely filled up the valley of the Stambach torrent. Since 1982 the torrent is again incising the material and has meanwhile reached depths of over 6 m in the lower parts.

The causes and history of the mass movement as well as the present geomorphology of the region are strongly related to its geological setting. The landscape is characterised by gentle slopes, built in the weak Triassic and Jurassic marls (Fleckenmergel) and Permo-Triassic salt clays (Haselgebirge), which are partly overlain by large and thick rigid slabs of Triassic and Jurassic Hallstatt Limestones and/or Dolomites (e.g. Tressenstein Limestone). Many of these slabs have disintegrated into smaller units that are moving apart in different directions. This process is called 'lateral spreading' (Varnes, 1978) or 'spreading' (Cruden and Varnes, 1996) and shown in Fig. 5.1 with an example (the Raschberg massif). The development of the Stambach earth flow is strongly related to spreading.

The slope, built in weak Haselgebirge and Fleckenmergel marls, is located down slope from and adjacent to the edge of one of these slabs, which consists of thick bedded limestones of the Tressenstein Formation, that dip to the North (around 40°NNW) and overlie the Haselgebirge discordantly. The base of this 80 m high and almost vertical rock face, called Zwerchwand, is destabilised due to the uphill propagating source area (which lies in the Haselgebirge) of the earth flow/creeping slope. As a result large rock pillars break down from the rock face (mostly by toppling) from time to time and collapse onto the upper part of the slope. Within the slope body, which consists of materials with a very low permeability (section 5.2) and which is almost completely saturated, excess pore water pressures are built up, leading to triggering of the earth flow. The most recent activation of the Stambach earth flow was caused by a rock pillar of around 30 000 m^3 collapsing onto the slope. The total volume of rock fall material deposited in

front of the Zwerchwand was estimated to be at least 600 000 m^3. Actually an approximately 20 000 m^3 rock pillar is toppling outwards the rock face with a velocity of around 12 $mm \cdot yr^{-1}$ (Rohn, 1991). Another factor contributing to disintegration of the Zwerchwand massif is the presence of a salt mine in a depth of around 700 m, within the underlying Haselgebirge directly below the northwestern part of the Zwerchwand, resulting in subsidence of overlying materials. However, the rock fall events causing the latest activation of the earth flow cannot be related to this as these occurred at the southeastern part.

The mechanism of activation as described above was first mentioned by Hutchinson and Bhandari (1971) who called it 'undrained loading'. In the Hallstatt region many earth flows are known having a similar triggering mechanism, e.g. the Sandling earth flow (1920), as shown in Fig. 5.1 (Rohn et al., 2004).

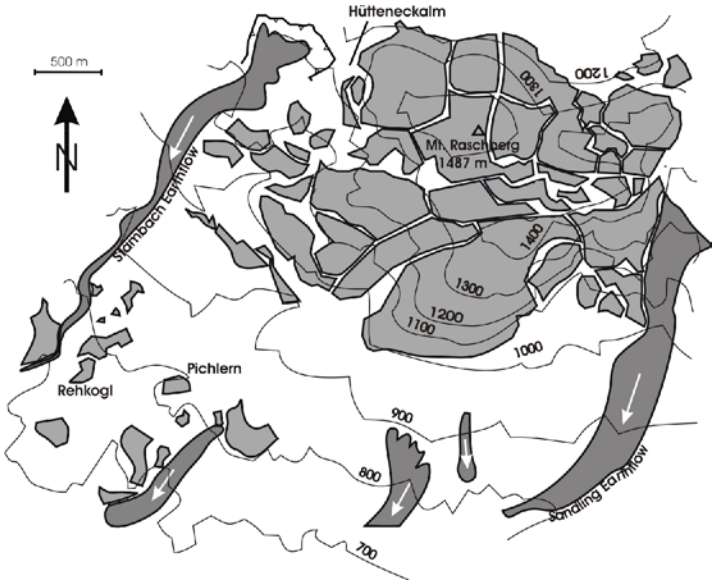

Fig. 5.1. Map of the area east of the Stambach slope, showing disintegration of the limestone slabs of the Raschberg Massif (grey) due to lateral spreading and showing the therewith related earth flows (dark-grey) (Rohn et al., 2004).

Besides from the mentioned source area at the foot of the Zwerchwand, the earth flow material is also delivered from a second main source area, located southeast of the Zwerchwand (indicated in Fig. 5.2). Contrary to the first source area, which is situated in Haselgebirge, this area is underlain by weathered Fleckenmergel marls. The slide mass therefore consists of Haselgebirge and Fleckenmergel, which in the upper part of the slope are found in unmixed form.

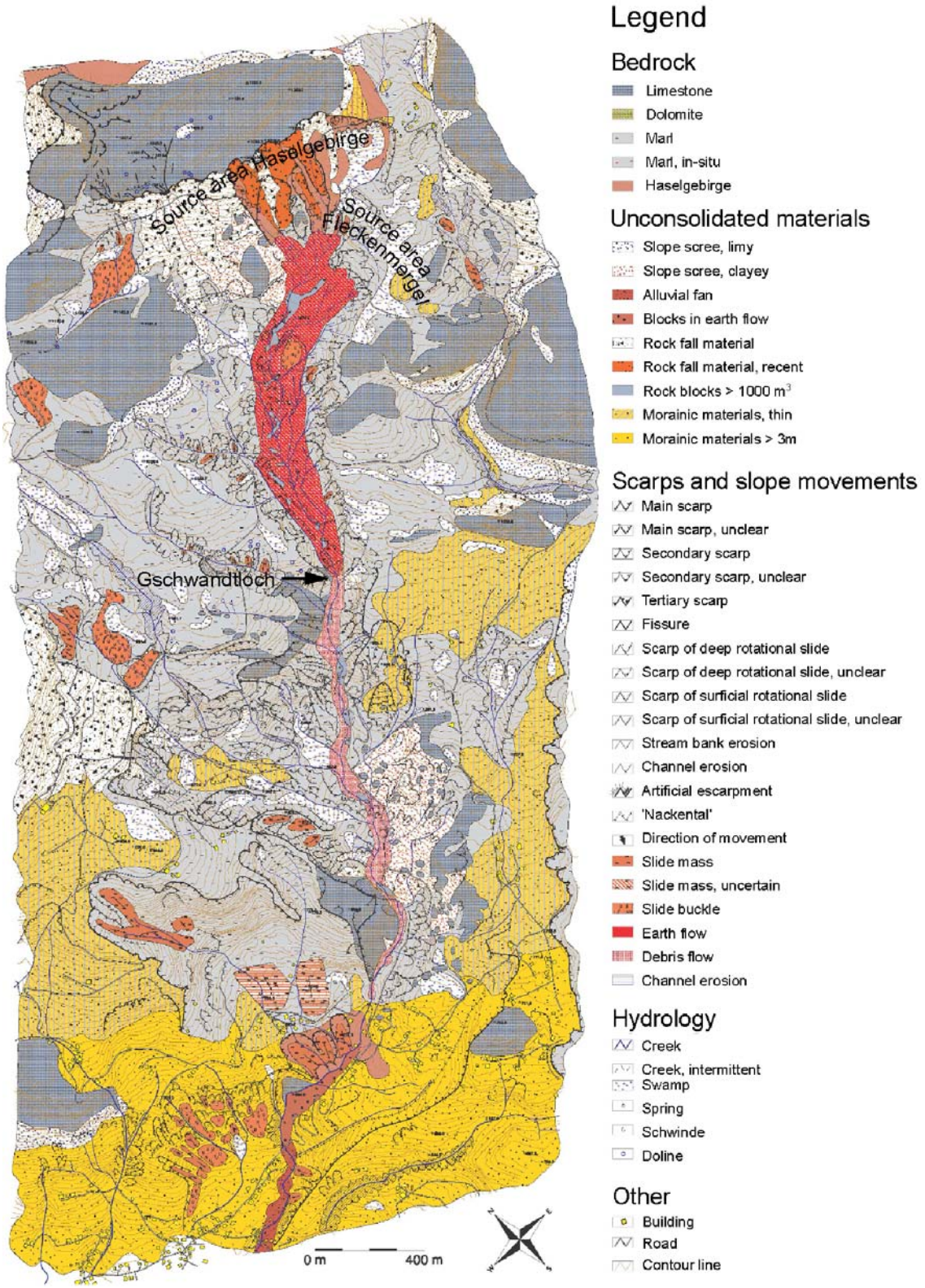

Fig. 5.2. Geotechnical map (after Rohn 1991, digitised by Fernandez-Steeger, 2002), with indication of the (presently inactive) earth flow and its two main source areas.

The northwestern part consists of Haselgebirge, the southeastern part of Fleckenmergel. Into a downhill direction the materials have been increasingly mixed.
The source areas, especially the southeastern one, appear as large depressions in the slope. During active phases of the earth flow they are 'emptied', resulting in a destabilisation of their back scarps. As a result, in these parts many small-sized slumps are activated, leading to the gradual expansion of the source areas.

During its last activation in 1982 the earth flow was initiated directly below the source area at the foot of the Zwerchwand, where around 10 months before the mentioned large rock pillar was collapsed. Within one month time, the movements had reached an around 1 250 m downhill situated narrow passage consisting of resistant limestones, called 'Gschwandtloch', by which the earth flow was temporarily blocked (see Fig. 5.2). Due to continuous supply of material from above, around 600 000 m^3 material could pass this bottleneck. Due to lateral supply of water from tributary torrents, with which the earth flow material was mixed, the earth flow translated into a much faster mudflow (Fig. 5.2). Within a period of only 24 hours the mudflow, which followed the course of the Stambach torrent into the direction of the Traun River, reached a second blockage, situated around 1 300 m downhill of Gschwandtloch. This bottleneck could not be passed by the mudflow anymore and marked therewith its end point. The presence of Haselgebirge and large blocks of Tressensteinkalk at the toe of the mudflow (at small distance of the Traun River) gives an indication of the huge distance (up to 2,5 km) over which large amounts of material must have been transported during previous active phases of the earth flow.

5.2 Slope geometry

Fig. 5.3 shows a site map of the study slope, which stretches from the Zwerchwand to 'Gschwandtloch' over a distance of around 1 250 m and has a maximum width of around 220 m. Six boreholes were logged through the slide mass into the stable basis of bedrock. The borehole records are shown in Fig. 5.5. Additional information about the depth of the bedrock was obtained by three seismic profiles across and one along the slide mass. Based on borehole information and seismic measurements the geotechnical model as shown in Fig. 5.4 was constructed. With an average thickness varying between 20 and 30 m, the volume of the moving mass was estimated at approximately $8 \cdot 10^6$ m^3.

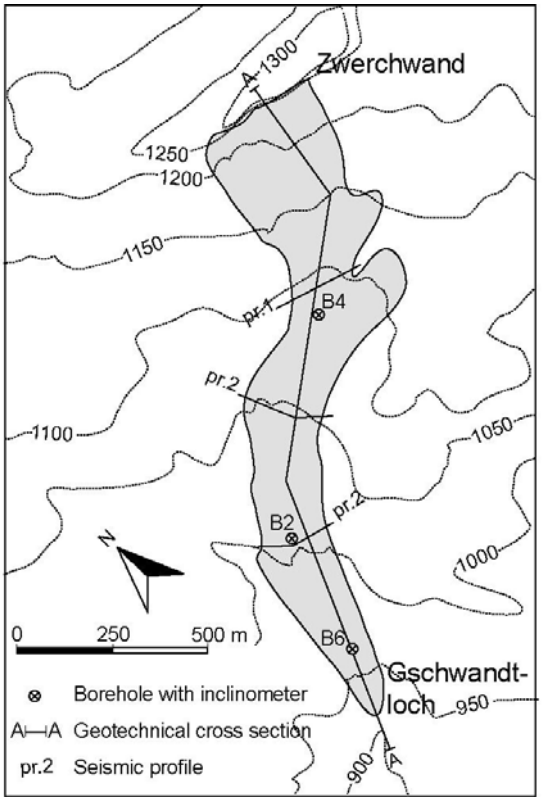

Fig. 5.3. Site map of the Stambach slope, with location of the boreholes (with inclinometer), seismic profiles and geotechnical cross section (after Rohn, 1991).

The average slope angle is around 10°. However, due to fine-scaled variability in slope profile the local inclination varies between 5° and 15°. The bedrock surface, forming the basis of the

creeping slope, runs roughly parallel to the slope surface and has approximately the same slope angle.

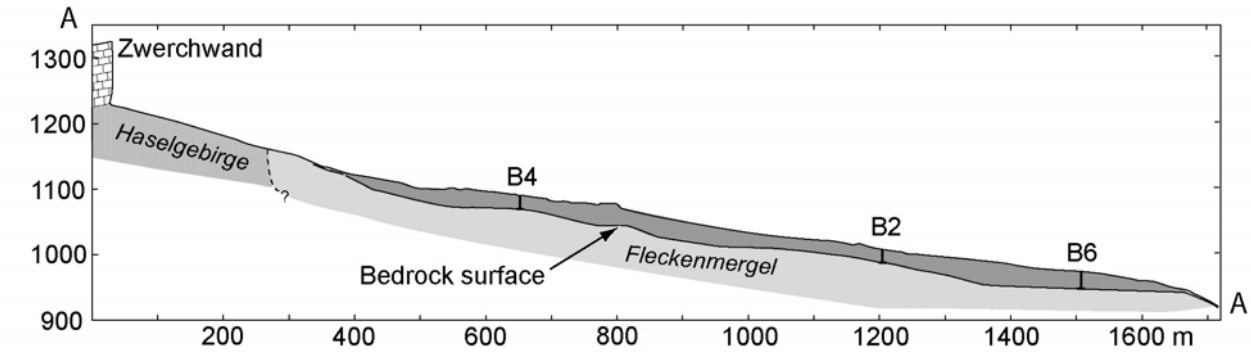

Fig. 5.4. Geotechnical cross section (location shown in Fig. 5.3) with locations of the boreholes in which inclinometer measurements were performed.

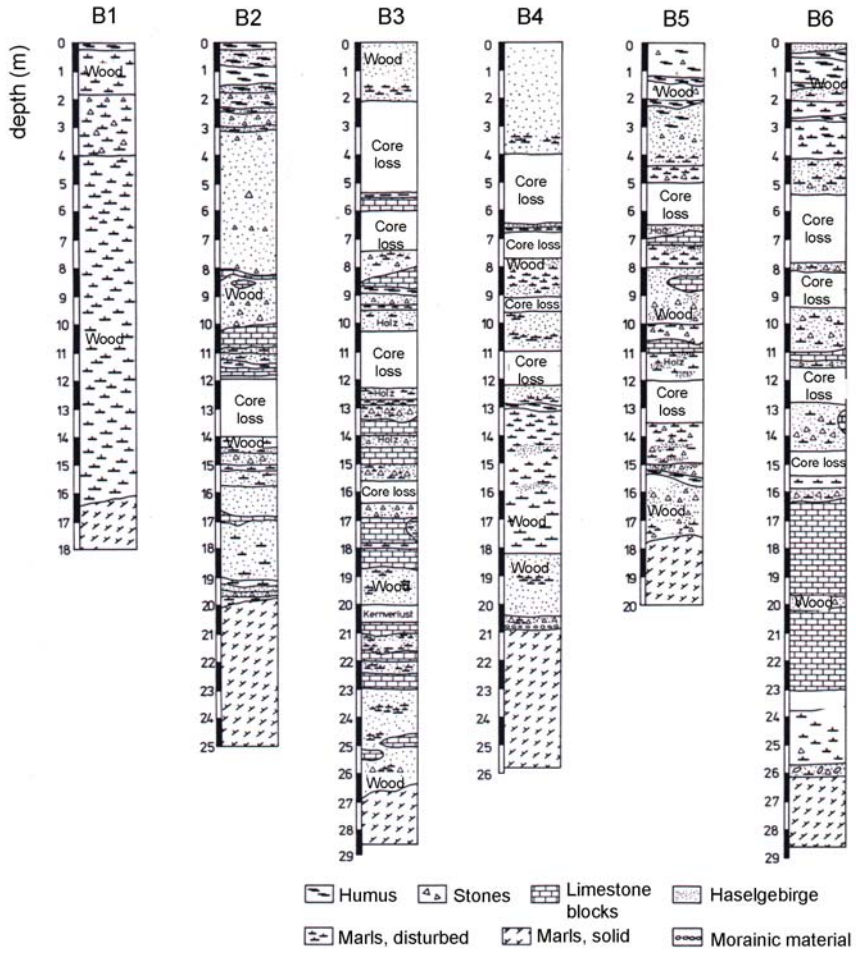

Fig. 5.5. Borehole records (locations see Fig. 5.11) (changed after Rohn, 1991).

5.3 Material characterisation

The slope body consists of the weathering products of the Fleckenmergel marls and the Haselgebirge claystones (in upper parts unmixed, in the lower parts mixed), which form a soil matrix in which occasionally some (unweathered) limestone blocks (Tressenstein Formation and limy parts of the Allgäu and Zlambach Formation) are embedded. However, as in general contact between these blocks is failing, it can be assumed that the mechanical behaviour of the slope solely depends on the properties of the soil matrix. The grain size distribution, shown in Fig. 5.6, shows that both materials are characterised by a relatively high clay content (Haselgebirge in average around 35% and Fleckenmergel around 45%).

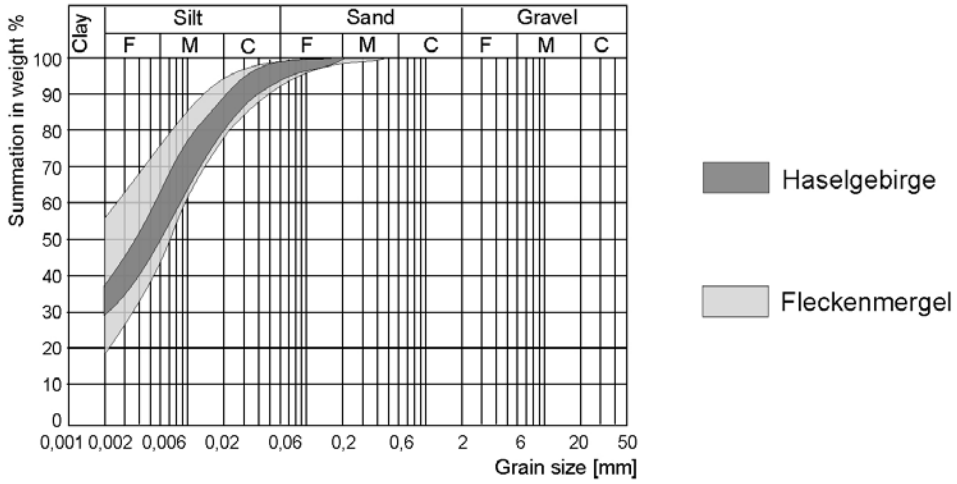

Fig. 5.6. Grain size distribution of Haselgebirge and Fleckenmergel.

Therefore the overall mechanical behaviour of both soil materials is for the major part determined by the behaviour of the clays. As explained in chapter 3 this behaviour is strongly determined by the type of clay minerals. From the slide mass a number of soil samples of both Haselgebirge and Fleckenmergel (in weathered form) were taken and tested semi-quantitatively on their mineralogical composition by means of X-ray diffractometer measurements on powder samples (non-textured, textured and saturated with ethylene glycol). The test results were compared with the results obtained by Rohn (1991) and Xiang (1997). It appeared that Fleckenmergel contains, in contrast to Haselgebirge, swelling clay minerals (mixed layer (i.e. smectite-illite) minerals) and carbonates.

Due to the presence of swelling clay minerals, the volumetric content of absorbed water in Fleckenmergel is higher compared to Haselgebirge (assuming that the slope is almost completely saturated). A higher content of absorbed water leads to an increase of plasticity (i.e. the difference between liquid limit w_L and plastic limit w_P increases). This is clearly shown in Table 5.1, which gives the Atterberg limits, and the plasticity chart in Fig. 5.7. A high plasticity does not only reduce the material's shear strength c_u, but also influences its viscous properties: according to the empirical relation in Eq. 3.16 viscosity index I_v increases with the liquid limit w_L. The presence of carbonates in Fleckenmergel, on the other hand, may cause cementation, leading to a higher shear strength and a reduction of plasticity. However, it can be expected that in surface-near depths the carbonates have been completely removed due to dissolution. This explains the lower plasticity of Fleckenmergel in unweathered form compared to its weathered form (Fig. 5.7).

The originally salt-bearing Haselgebirge has been leached out completely.

Table 5.1. Atterberg limits for Haselgebirge and Fleckenmergel: liquid limit (w_L), plastic limit (w_P) and plasticity index ($I_P = w_L - w_P$).

	w_L [%]	w_P [%]	I_P [-]
Haselgebirge	36,5±3,5*	21,2±0,6*	15,2±3,6*
Fleckenmergel	66,5±7,5*	29,5±2,3*	37,0±7,8*

*The first value is the average of around 10 samples, tested by Rohn (1991), Xiang (1997) and own tests. The second value is the standard deviation, which calculation is allowed as the values appeared to be normally distributed.

Compared to Haselgebirge, Fleckenmergel is characterised by a relatively high plasticity index (I_P), which means that for Haselgebirge the amount of water, required to change its state from a semi-solid into a liquid, is smaller.

Table 5.2. Soil classification values: void ratio (e_0), grain unit weight (γ_s), dry unit weight (γ_d) and buoyant unit weight (γ_b).

	e_0 [-]	γ_s [kN·m^{-3}]	γ_d [kN·m^{-3}]	γ_b [kN·m^{-3}]
Haselgebirge	1,4	26,9	11,1	7,1
Fleckenmergel	1,2	26,3	11,8	7,5

Table 5.2 shows void ratio (e_0), grain unit weight (γ_s), dry unit weight (γ_d) and buoyant unit weight (or submerged unit weight) (γ_b) of both materials.

The same material used for determination of the values shown in Tables 5.1 and 5.2 was used for the laboratory tests that will be presented in chapter 6.

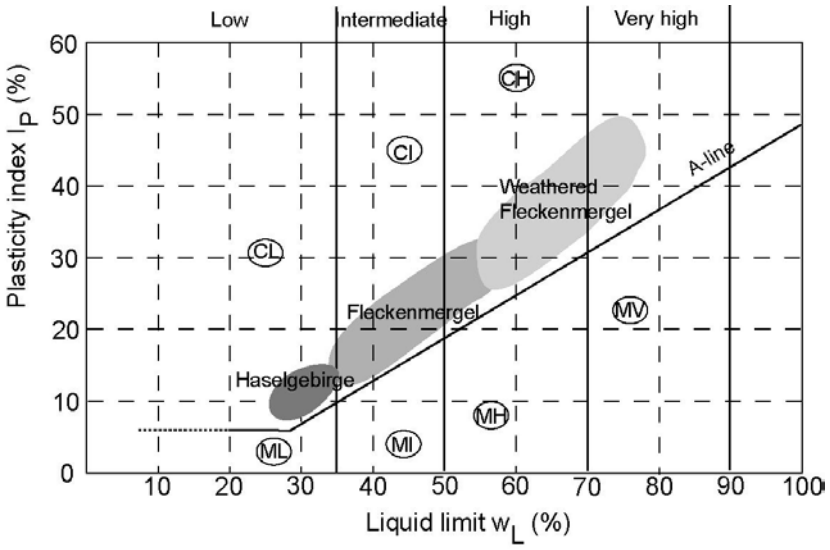

Fig. 5.7. Classification of Haselgebirge and Fleckenmergel (both weathered and unweathered) in the plasticity chart of Casagrande. C stands for clay (above the A-line), M stands for silt (below the A-line). V, H, I and L indicate very high, high, intermediate and low plasticity respectively (based on own tests and values from Rohn (1991)).

Both materials have a very low hydraulic permeability. Rohn (1991) determined coefficients of hydraulic permeability (for water) for Fleckenmergel and Haselgebirge to be approximately $8 \cdot 10^{-11}$ $m \cdot s^{-1}$ and $3 \cdot 10^{-11}$ $m \cdot s^{-1}$ respectively, which means that the materials are practically impermeable. However, these values apply to soil samples tested in the laboratory, which means that natural heterogeneities, especially the presence of fissures, within the slope body were not accounted for. Therefore it can be assumed that the overall permeability of the slope body is higher. Overall permeability measurements were not available, but could be obtained by means of in-situ permeability tests (pump-well or pumping-in tests).

5.4 Field measurements

The field measurements, which all started in 1988, comprise of measurements of the slope movements by inclinometers in the boreholes at the one hand and pore water pressure measurements by piezometers and determination of free water tables in the (inclinometer) boreholes at the other hand.

5.4.1 Inclinometer measurements

In three boreholes inclinometers were installed, with which the horizontal displacements in the direction of the steepest descent were measured over a period of 16 years. As all boreholes were drilled at least 5 meters into the stable bedrock, the foot of the inclinometers can be assumed to be fixed. Fig. 5.8 and Fig. 5.9 show the results for boreholes B2 and B4 respectively (the results from borehole B6 appeared to be unusable). Both absolute displacements (a) and relative velocities (b) over depth are shown. With the latter the difference in velocities between two points at 1 m vertical distance is meant. Usage of relative velocities enables comparison of measured velocities with velocities simulated with the model at different depths independently of each other (i.e. corrected for spatial autocorrelation of the data points along the borehole). It can be seen that for both B2 and B4 fluctuations in relative velocity over depth are rather small. This indicates the absence of clear shear zones. The slightly higher deformation rates between 15 and 20 m in B2 could be explained by the presence of a confined aquifer at the basis of the creeping mass, which was indicated by small amounts of water welling up at the surface as the basis was reached during drilling (see next section).

The relatively large displacements, observed in the upper 2 m of both boreholes, can be explained by alternating wetting-desiccation and consequent swelling-shrinkage of the surface-near and unsaturated topsoil. As these processes, which are directly related to the alternation of rainfall periods with dry periods, occur independently of the main creep movements, they were not considered in the simulations described in chapter 6.

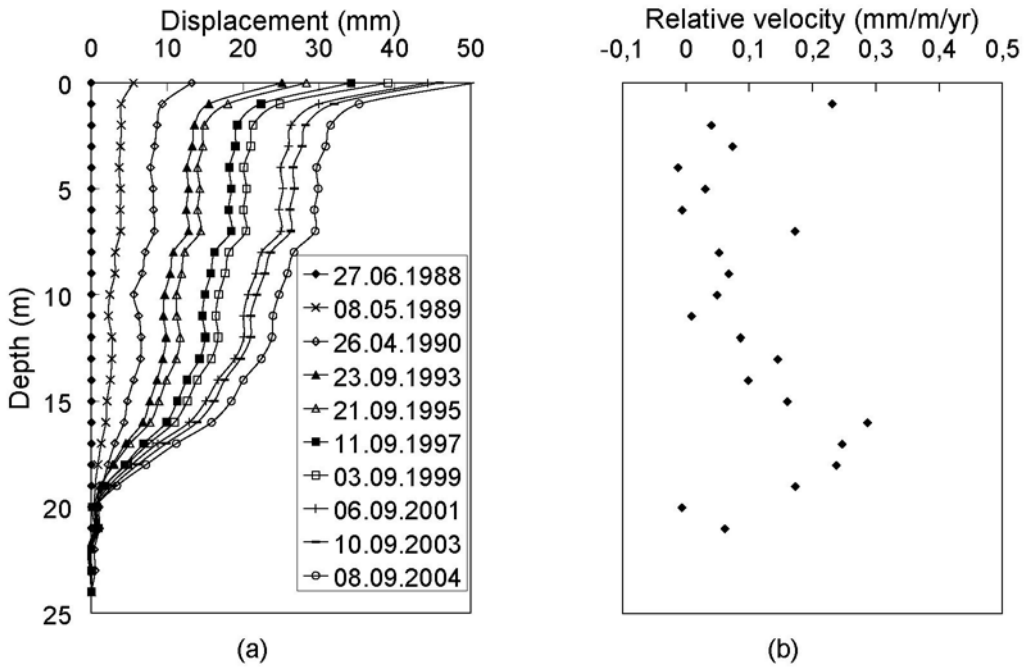

Fig. 5.8. Inclinometer results for borehole B2, with displacements (a) and relative velocities (b).

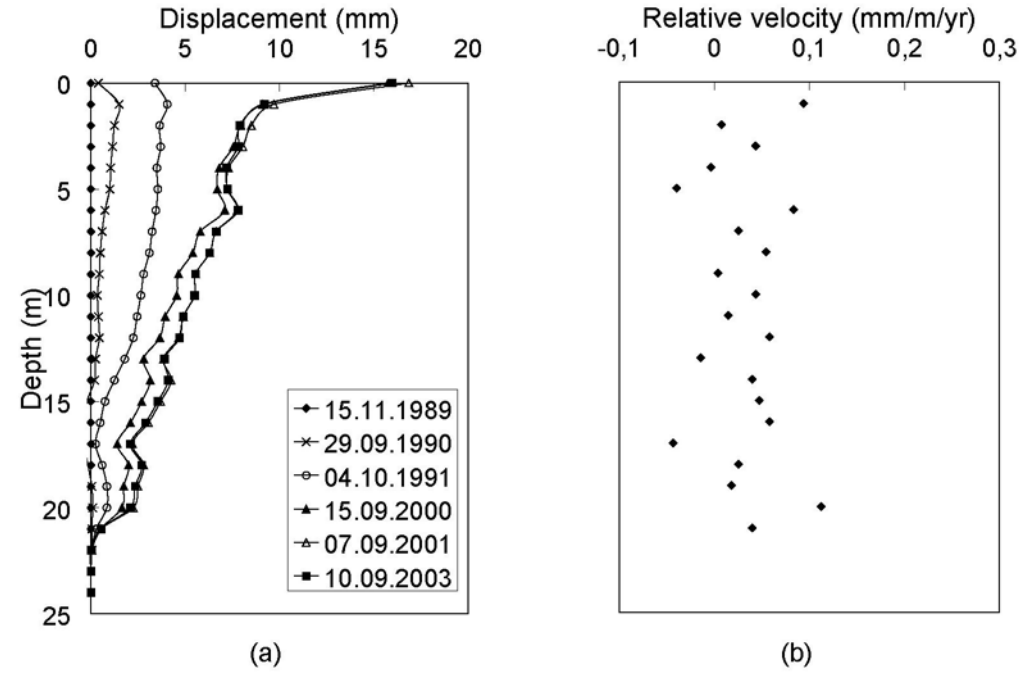

Fig. 5.9. Inclinometer results for borehole B4, with displacements (a) and relative velocities (b).

Fig. 5.10 shows the evolution of relative velocity over time. Because of the lack of a clear trend in change of relative velocity over depth, the depicted values represent relative velocities that are

averaged over the total borehole length (except for the upper 2 m). In both locations the relative velocity decreases slightly over time. This is also demonstrated by the plotted (logarithmic) regression lines, which show that also deceleration is not constant, but diminishes over time. The deceleration rate is for both locations very similar. In B2, however, the average relative velocity is about three times higher than in B4. The difference could be explained by the mentioned fine-scaled variability in slope angle (of both slope surface and basis of the creeping slope body). In the field an alternation of zones of contraction with zones of distraction can be observed, which' location can clearly be related to the local slope angle. The slope angle in B4 is slightly smaller than in B2 (see Fig. 5.4).

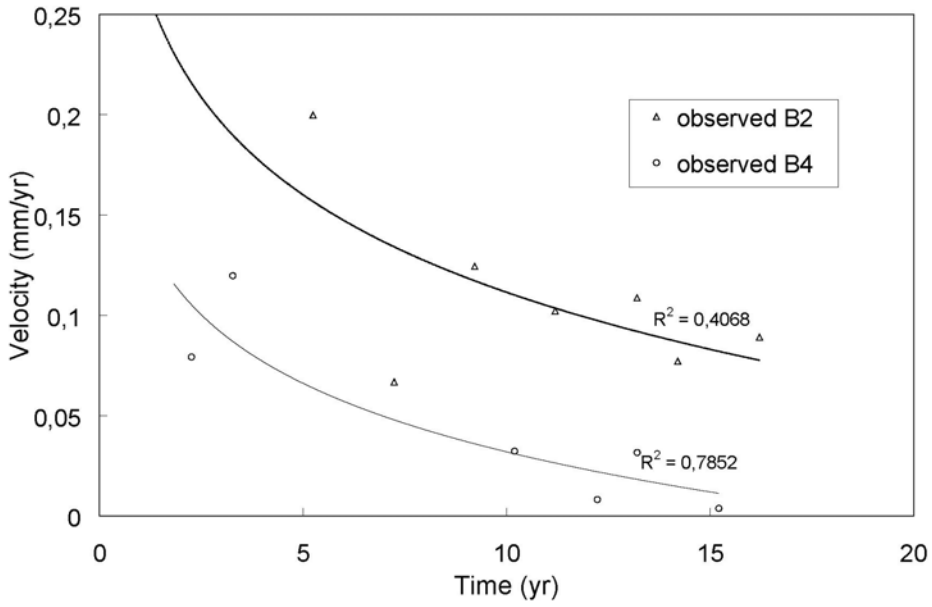

Fig. 5.10. Change of relative velocity over time for boreholes B2 and B4 with logarithmic regression lines and goodness of fit.

The measurements had a time-interval of 1 year, so that seasonal variations could not be accounted for. However, pore water pressures within the slope body, which can be considered to be the dominant controlling factor of the velocity of the creep movements, appear to be rather stable over the year, as will be further explained in the next section. Therefore it can be assumed that seasonal variations of the deformation velocities will be small as well.

5.4.2 Pore water pressure measurements

Pore water pressures within the slope body were determined by means of piezometer measurements as well as free water tables in the boreholes. Piezometers were installed in three boreholes (B1, B3 and B5) at different depths and were continuously operative over a period of two years. Fig 5.11 shows the results, including the annual variations in case of piezometer measurements. Both pore water pressures obtained from piezometers and free water tables in the boreholes indicate a surface near phreatic level. Comparison between rainfall and piezometer measurements within the slope mass showed that pore water pressure, even in small depths, hardly reacts to rainfall, which can be ascribed to the low permeability as well as the high degree of saturation of the slope materials. In-situ infiltration experiments showed that 90-95% of the supplied water discharged by means of runoff (oral communication with Rohn, 2005).

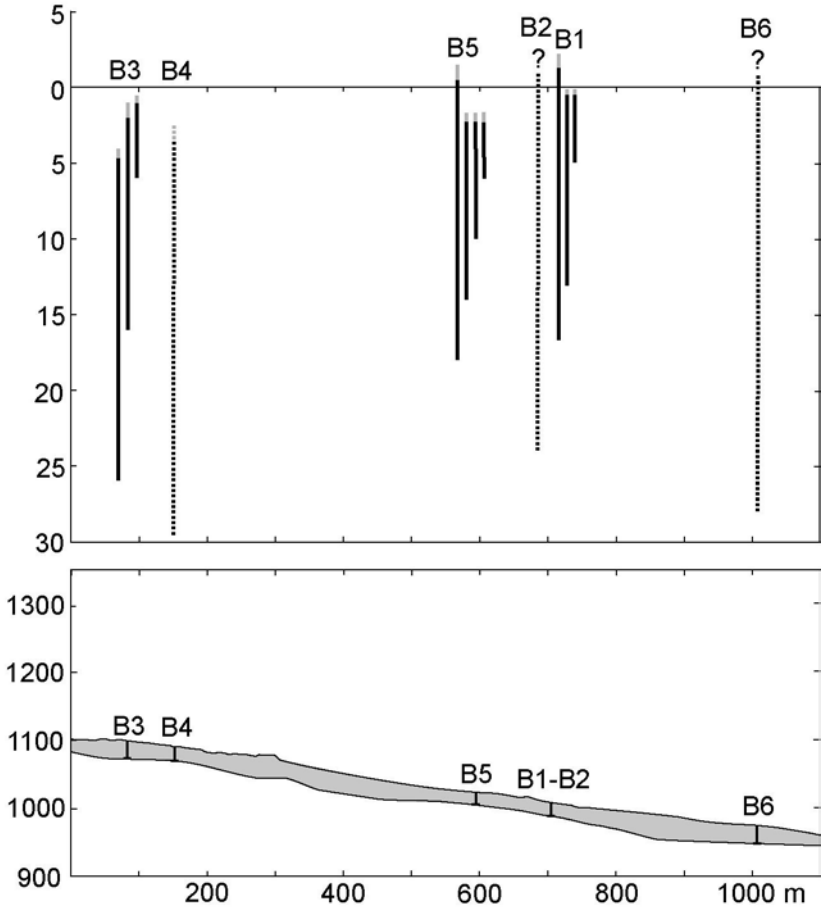

Fig. 5.11. Spatial distribution of the pore water pressure, expressed in heads (m) relative to the slope surface (upper diagramme). Dotted lines represent free water tables in inclinometers, continuous lines represent piezometer measurements in indicated depths, grey parts of the line indicate the annual variations (after Rohn, 1991).

The lowermost piezometers in B1 and B5, that were installed at the basis of the slide mass, as well as the small amounts of water welling up in the inclinometer tubes in B2 and B6 showed the presence of excess pore water pressures at the basis of the middle part of the slope. As in the basal parts of the slope sections uphill to this section normal (i.e. hydrostatic) pore water pressures were measured, this could indicate the presence of an artesian aquifer, which stretches from the boundaries to the basal parts of the slope.

Chapter 6 Numerical simulation of the Stambach slope

6.1 Introduction

This chapter shows the application of the visco-hypoplastic law for predicting the slope deformations of the Stambach slope. Using the slope data presented in chapter 4 and 5, the theory of simulation of creep movements (i.e. behaviour of clay soils and the visco-hypoplastic law) and the methods for tackling the problem of limited availability of subsurface data (particularly material heterogeneity and initial state variables) as presented in Part 1, were applied and tested for their validity.

Section 6.2 deals with the sampling strategy and the determination of the material parameters by means of oedometer and triaxial tests, according to the theory that was given in section 3.3. In section 6.3 it is tested whether the visco-hypoplastic law holds for the soils studied by simulating the laboratory tests with an element test programme. Section 6.4 and 6.5 show the simulation of the slope movements using the same element test programme and the FE-programme Abaqus respectively, according to the methodology given in section 4.2. Here it is described in which way the available subsurface information concerning slope geometry, material heterogeneity, pore water pressure distribution and initial state variables were incorporated.

In section 6.6 the simulation results are discussed and the quality of the models for prediction slope deformations is evaluated. By means of sensitivity analyses the influence of uncertainties of a number of parameters on the model performance was quantified by varying them between expected ranges. Finally some explanations are given for differences in simulation results between the element test and FE-model.

A final evaluation of the suitability of the applied methodology and the visco-hypoplastic material law for prediction of creep movements will be given in chapter 7.

6.2 Determination of the visco-hypoplastic material parameters

6.2.1 Sampling and preparation of the samples

Although slope materials of the Stambach slope show a strong heterogeneity, only a limited number of laboratory tests could be performed, due to their high cost and time-demands. While in the upper part of the slope the two source materials are found in unmixed form, in its lower parts the materials have been increasingly mixed. For this reason material parameters were determined on samples of Haselgebirge and Fleckenmergel in unmixed form, in order to comprehend the expected range of material parameters as good as possible. The soil material was taken near the slope surface by excavation.

In order to verify whether the samples taken were representative for Haselgebirge and Fleckenmergel in unmixed form, their mineralogical composition was investigated by means of X-ray diffraction measurements. The results were discussed in section 5.2.

Oedometer and triaxial tests were performed on disturbed, homogenised soil material, having a water content approximately equal to the liquid limit (Table 5.1). This way the presence of irregularities, which may influence the test results, could be excluded and a degree of saturation of approximately 1 could be achieved. Furthermore, all tests could be performed on the same material, by which it was possible to compare their results which each other. The classification values of the samples before they were tested (i.e. void ratio and weights) are given in section 5.3 (Fig. 5.6 and 5.7 and Table 5.1 and 5.2).

6.2.2 Oedometer tests

In order to determine the compressibility index λ, swelling index κ and e_{100} (void ratio during isotropic compression with referential strain rate $\dot{\varepsilon}_r$ at 100 kPa), oedometer tests were performed, in which axial load was incrementally increased (Incremental Loading (IL)-test).

Fig. 6.1 shows the σ-e-graphs of the IL-tests performed on Haselgebirge and Fleckenmergel respectively (initial void ratios are given in Table 5.2). In total five load increments were applied. Each point represents the void ratio e at the End of the Primary Consolidation (EOP) due to the applied axial effective stress (σ_1'). As EOP represents the onset of the creep phase, this means that both straight lines in Fig. 6.1 represent the primary consolidation lines, in which OCR=1. If each load increment would have been preceded by a creeping phase, the e-$\ln\sigma_1'$ states would lie on a lower positioned isochrone (see Fig. 3.2).

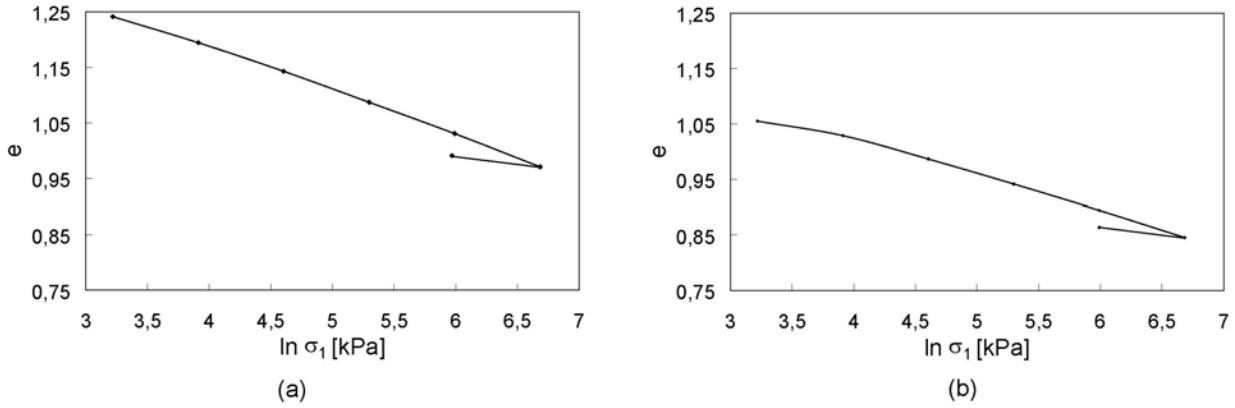

Fig. 6.1. Oedometric IL-test results for Haselgebirge (a) and Fleckenmergel (b).

After EOP of the last load increment was reached, the sample was unloaded by removal of the final load increment. From the loading and unloading branches of the curves in Fig. 6.1 λ and κ were determined respectively.

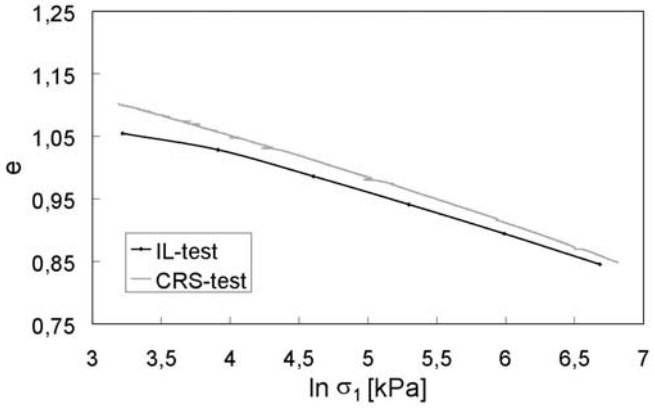

Fig. 6.2. Comparison between oedometric IL-test and CRS-test results for Fleckenmergel.

In theory, compression of a sample of the same material as used in the IL-test with a strain rate equal to the strain rate at EOP in the IL-test should yield e-$\ln\sigma_1'$ states that lie on the same isotach as shown in Fig. 6.1. In order to prove this theory, a (drained) constant rate of strain test (CRS-test) was performed on a Fleckenmergel sample. Fig. 6.2 shows the comparison between the results of the IL- and CRS-tests, showing a slightly higher position of the line obtained by the CRS-test. This could be explained by a too high strain rate, implying that excess pore water pressures had developed within the sample. Therefore, the material parameters κ, λ and e_{100} were determined from the primary consolidation lines obtained by the IL-tests as shown in Fig. 6.1 (according to the method shown in Fig. 3.2) and the strain rate calculated at the EOP was used as referential strain rate $\dot{\varepsilon}_r$.

6.2.3 Triaxial tests

In order to determine the critical friction angle φ_c and viscosity index I_v, on both samples strain rate controlled CU (consolidated undrained) triaxial tests with a jump in strain rate were performed. During the tests pore water pressure within the sample was measured.
First the samples were consolidated oedometrically until EOP was reached. Then they were installed in the triaxial apparatus and consolidated isotropically, again until EOP. By means of a saturation test it was verified if the degree of saturation within the samples was (nearly) 1.
Shearing took place with a cell pressure of 100 kPa. The test was started with an axial strain rate of 0,005 mm·s^{-1}. Having reached an axial strain of around 5% (axial strain ε was explained by Fig. 3.1), the strain rate was increased to 0,052 mm·s^{-1}. Finally strain rate was brought back to its initial value and the test was finished.
The results for Haselgebirge and Fleckenmergel are shown in Fig. 6.3 and Fig. 6.4 respectively, with in both figures on the left the stress path and on the right the ε-q-curve, (q and p' were defined in section 3.2). φ_c was obtained from the stress path, using Eq. 3.13 (see also Fig. 3.5(a)). I_v was determined from the ε-q-graph, using Eq. 3.15.

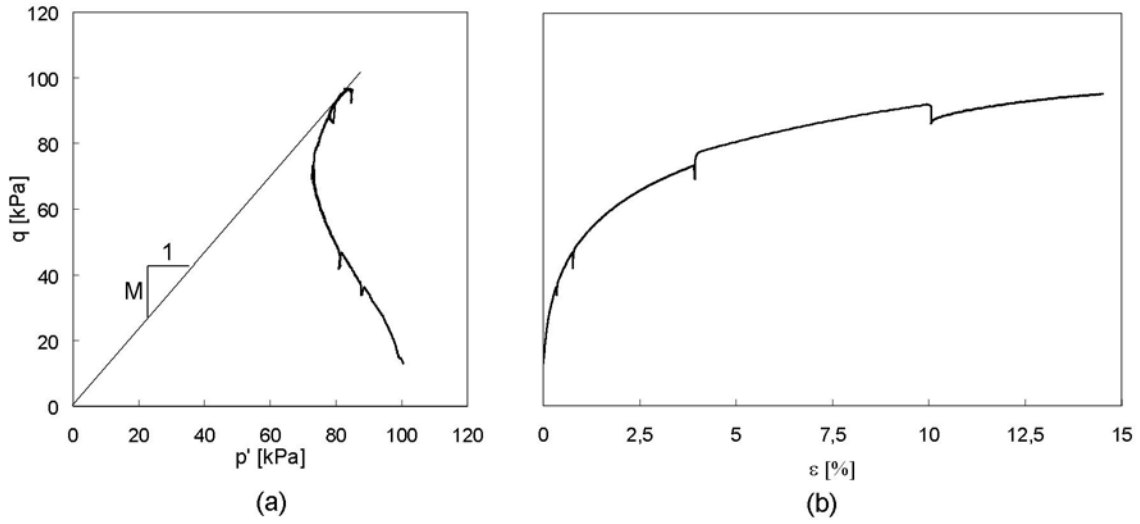

Fig. 6.3. Results of a triaxial test performed on a Haselgebirge sample, with stress path (a) and stress-strain curve (b). (irregularities are due to small discontinuities in compression rate).

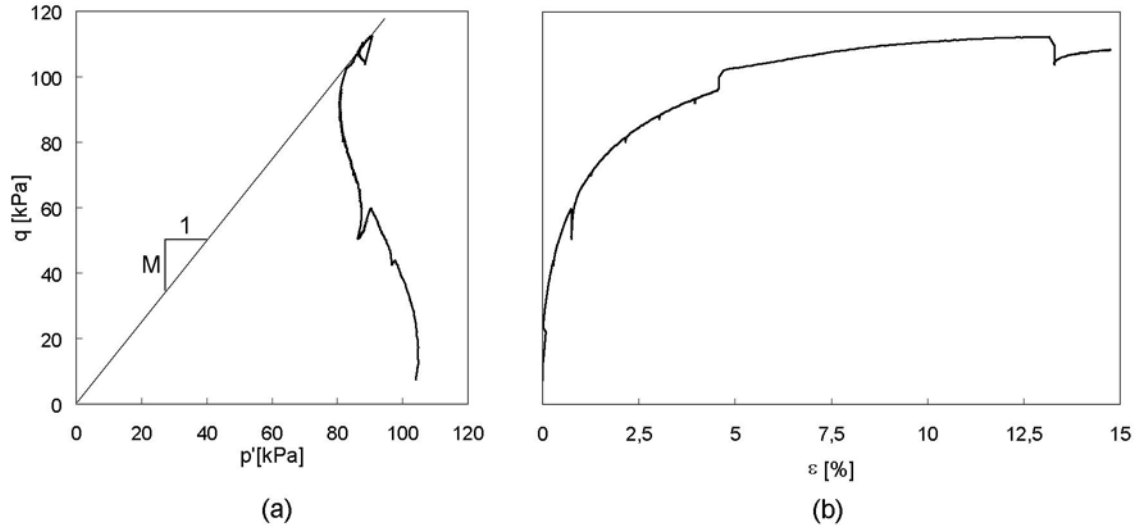

Fig. 6.4. Results of a triaxial test performed on a Fleckenmergel sample, with stress path (a) and stress-strain curve (b).

6.2.4 Summary and discussion of the visco-hypoplastic material parameters

Table 6.1 shows the obtained set of material parameters for Haselgebirge and Fleckenmergel. The very small values of I_v, κ and λ are in agreement with the classification of both materials to be clays of low to intermediate plasticity (see Fig. 5.7). However, in case of Fleckenmergel the small values indicate that the sample material did possibly not represent the completely unweathered

material (of which the slide mass is expected mainly to consist of). This could be explained by the fact that the samples were taken close to the edge of the earth flow, where the degree of weathering might be smaller (oral communication with Rohn, 2005). (Table 5.1 already indicated the rather large variability of Fleckenmergel). The higher carbonate content of Fleckenmergel in less weathered form leads to a lower plasticity. An alternative explanation for the possibly too small values may be an incomplete adsorption of innercrystalline water by the swelling clays within the sample during the tests, which is not reflected by the saturation test. Since the sample material was taken close the surface, where it can be assumed that the soil is only partly saturated, the material had to be saturated in the laboratory subsequently. The time allowed for saturation may have been too short. As explained in chapter 3, the amount of water adsorbed by the clay particles influences the behaviour of the material strongly.

The maximum shear strength c_u (calculated from q_c in Fig 6.3 and Fig. 6.4 with Eq. 3.14) is for Fleckenmergel around 1,5 times higher than for Haselgebirge. Since the critical friction angle φ_c of the latter is slightly larger, the differences in maximum strength can be ascribed to different initial OCR's for both materials.

Table 6.1. The visco-hypoplastic material parameters for Haselgebirge and Fleckenmergel.

	e_{100} [-]	λ [-]	κ [-]	φ_c [°]	I_v [-]	$\dot{\varepsilon}_r$ [s^{-1}]
Haselgebirge	1,13	0,031	0,0041	31,1	0,014	7,6E-6
Fleckenmergel	0,96	0,037	0,0045	28,4	0,016	7,6E-6

6.3 Simulation of the element tests

In order to test whether the visco-hypoplastic material law holds for the soils studied, the oedometer and triaxial tests were simulated with an element test programme in which the visco-hypoplastic law was implemented, using the material parameters presented in Table 6.1.

As the viscous behaviour of soil depends on stress, void ratio, deformation rate and history of velocity, realistic back-prediction of the laboratory tests requires simulation of the complete sequence of loading and strains. For example, in case of the triaxial test, both oedometric and isotropic consolidation, including possible creep phases, should also be simulated in order to enable a sound comparison with the experimental results.

The IL-oedometer tests were simulated by considering them as a CRS-test. This is justified if the calculated strain rate at EOP is used, which corresponds to the referential strain rate $\dot{\varepsilon}_r$ in Table 6.1. Fig. 6.5 shows the e-$\ln\sigma_1'$ curves obtained by experiment and simulation. Initial void ratio was set equal to the void ratio determined on the uncompressed material before it was installed into the oedometer box (i.e. the values of e_0 in Table 5.2). As can be seen, for both materials the simulation results fit rather well with the observations.

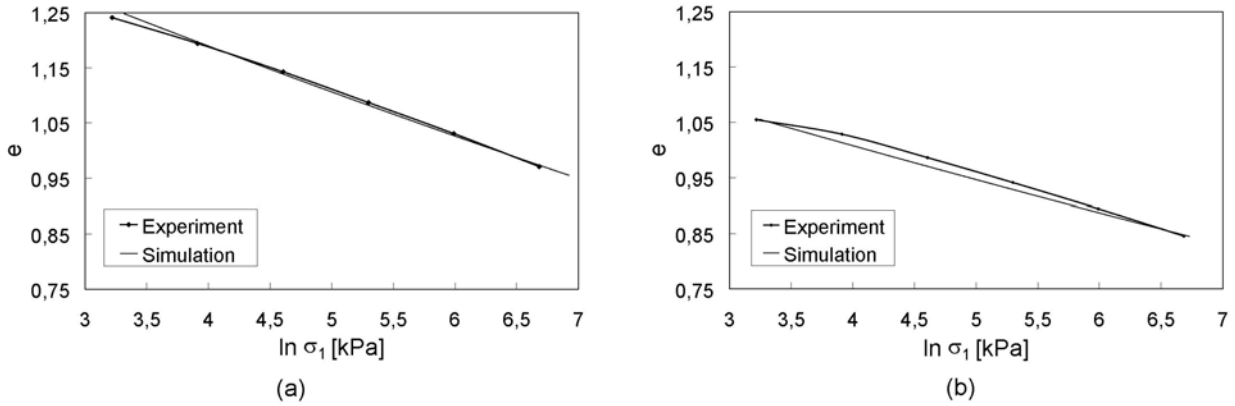

Fig. 6.5. Comparison between simulation and experiment for the oedometric IL-tests performed on Haselgebirge (a) and Fleckenmergel (b) samples.

Fig. 6.6 and 6.7 show a comparison between the observed and simulated results of the triaxial tests performed on Haselgebirge and Fleckenmergel respectively.

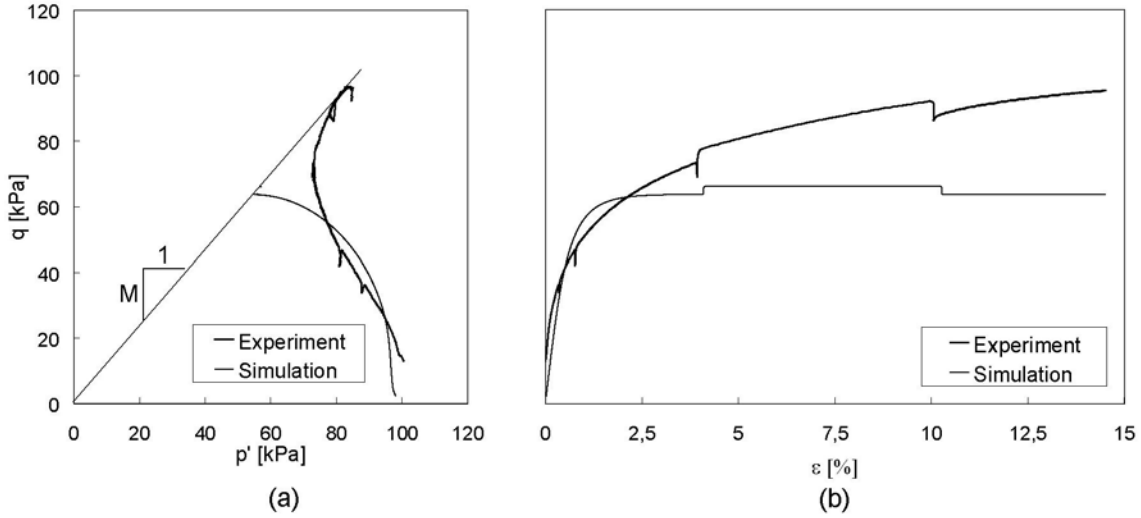

Fig. 6.6. Comparison between simulation and experiment for the CU triaxial test performed on a Haselgebirge sample, with stress path (and critical state line) (a) and stress-strain curve (b).

Also the jumps in strain rate were simulated (indicated by the two breaks in the stress-strain curve). Up to axial strains of approximately 3%, simulation results fit rather well with the observations for both materials. For larger strains, however, both simulated stress path and stress-strain curve start to deviate significantly from the experimentally assessed ones. This can be explained by inaccuracies of the triaxial test. Bulging of the sample during axial compression, caused by friction between the soil sample and base and load plates, results in heterogeneities in stress distribution. This results in increasing deviations in the experimentally obtained curve with increasing strains. Nevertheless φ_c determined from the simulated stress path is similar to φ_c determined from the experimental one, as the critical state lines coincide.

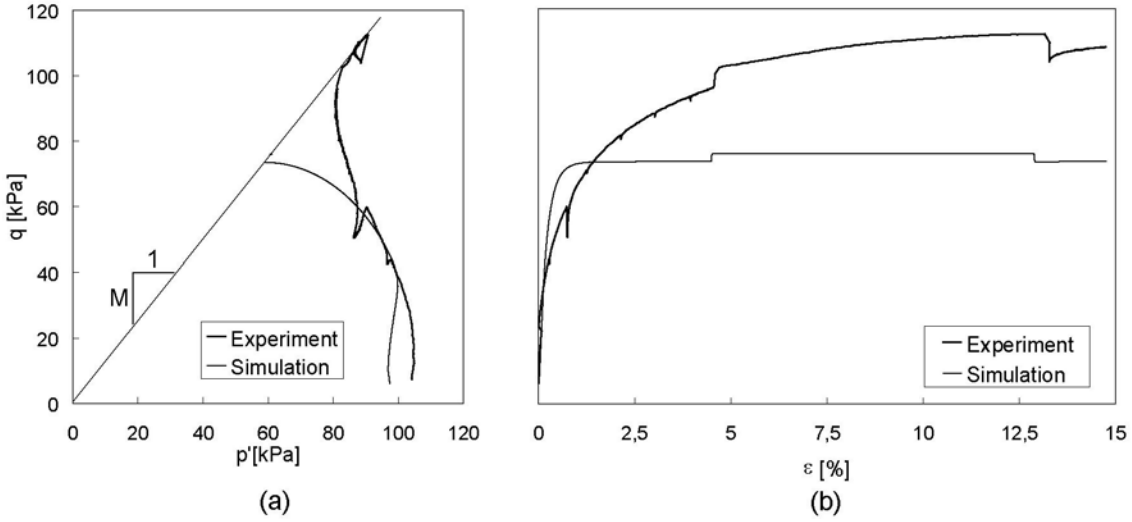

Fig. 6.7. Comparison between simulation and experiment for the CU triaxial test performed on a Fleckenmergel sample, with stress path (and critical state line) (a) and stress-strain curve (b).

In Fig. 6.8 the simulated evolution of OCR during the course of the tests is shown. In both cases an OCR of approximately 1 is reached rapidly. The jump to the approximately 10 times higher strain rate only leads to a small reduction of OCR, which can be explained by the relatively small I_v for both materials (see Eq. 3.6).

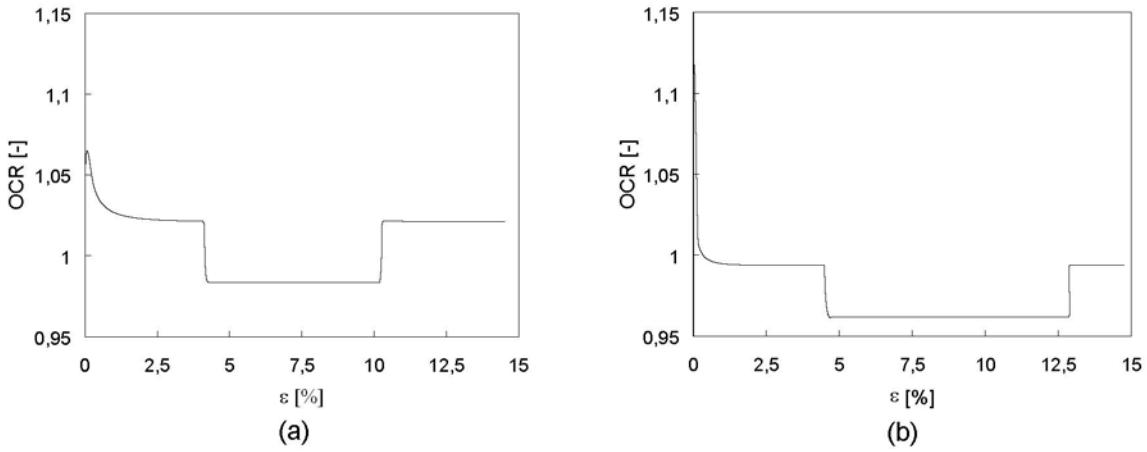

Fig. 6.8. Evolution of OCR during CU triaxial test performed on Haselgebirge (a) and Fleckenmergel (b).

6.4 Simulation of slope deformations with an element test model

The same element test programme with which the laboratory element tests were simulated, was used for simulation of the slope movements. The results were compared with relative velocities which were calculated from the inclinometer measurements (Fig. 5.8(b) and Fig. 5.9(b)). Besides spatial autocorrelation (section 5.4.1), the use of relative velocities also excludes temporal autocorrelation, in contrary to absolute displacements. The results were also published in Van den Ham et al. (2005a).

6.4.1 Initial and boundary conditions

The slope movements were simulated on relatively small soil segments of 1 m (vertical) thickness, which were considered as parts of an infinite slope (Fig. 6.9). The assumption of an infinite slope is justified by the very small thickness/length ratio of the creeping slope. A first reason for using the relatively small element size was to minimise the influence of the simplification that within a single element state variables and material parameters are assumed to be homogeneous. Furthermore, it enables an easy comparison with the relative velocities calculated from the inclinometers (Fig. 5.6 and Fig. 5.9), as these represent the differences in velocity between two points at 1 m (vertical) distance as well (for this reason a smaller element

size would not make sense). In order to analyse fields of displacements and velocities, slope segments at different depths were simulated.

Based on the piezometer measurements and free water table in the boreholes (see section 5.4.2) the phreatic level was assumed to be at the surface and the slope body to be completely saturated. This was incorporated into the model by performing the simulations using effective stresses.
An initial stress state had to be estimated, as no field measurements were available. Vertical effective stress (σ'_v) acting on a soil segment was calculated from its depth below the surface multiplied with the buoyant weight of the overlying soil material. As no quantitative data concerning the artesian layer at the base of the creeping mass were available, it was not accounted for in the simulation. Buoyant weight γ_b was assessed at 7,3 kN·m^{-3} by averaging the buoyant weights determined on Haselgebirge and Fleckenmergel (see Table 5.2).
For calculation of the horizontal effective stress (σ'_h) the initial coefficient of earth pressure at rest K_0 was approximated with the equation of Jaky (Eq. 3.17). The shear stress was calculated from the slope angle and the vertical stress.

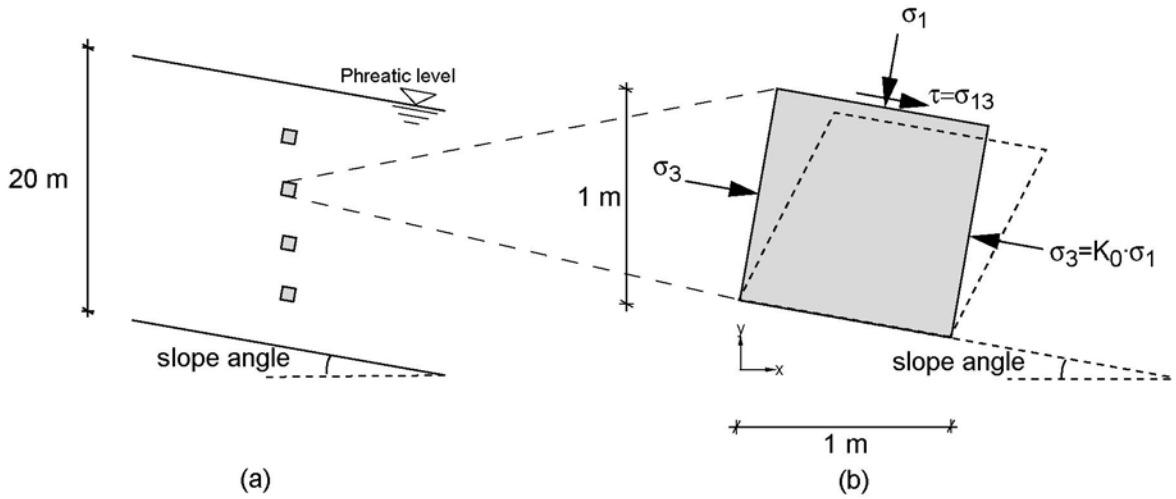

Fig. 6.9. Boundary conditions of the element test model. Assumed is an infinite slope (a), in which slope deformations at slope sections of 1 m thickness at four depths were calculated (b).

Although pore water flow may occur in zones of non-uniform distributed pore water pressures, the lack of data concerning the overall permeability of the slope body (see section 5.3) made simulation with a pore water flow model (which could be coupled to the mechanical model) meaningless. Therefore, in this study a model was used that only accounted for either drained or

undrained conditions. Despite of the expected very low overall permeability of the slope materials, it was decided to use a completely drained model. The application of fully undrained conditions would lead to high excess pore water pressures, building up during the initial stages of simulation, which cannot dissipate afterwards. This would not be in agreement with the piezometer measurements, as these did not reveal excess pore water pressures. This also implies that possible volumetric creep has apparently not led to the development of excess pore water pressures either.

Initial void ratio can be set as an initial value or can be calculated by the visco-hypoplastic law for a given OCR. No direct measurements of the density distribution within the slope were available for verification. However, assuming a degree of saturation of the slope to be approximately equal to 1, the decrease of void ratio over depth could be estimated from the change in water content over depth, which was determined on soil samples from the borehole record at different depths.

The calculation was then performed in two steps. First the aforementioned stresses acting on the element were built up relatively rapidly. Then creep movements were calculated by keeping the stresses constant.

The simulation results were finally compared to the relative velocities that were calculated from the inclinometer measurements. Due to the fact that these inclinometer measurements started in 1988, so around 6 years after the last activation of the earth flow, no information about the deceleration history up to the measured deformation rates is available. These first 6 years were also simulated with the model, but were left out in the comparison of the results with the measurements.

6.4.2 Results

Fig. 6.10 shows the simulated decrease of void ratio, using an initial OCR of 1,5, compared with the observed decrease of void ratio obtained according to the method described in the previous section.

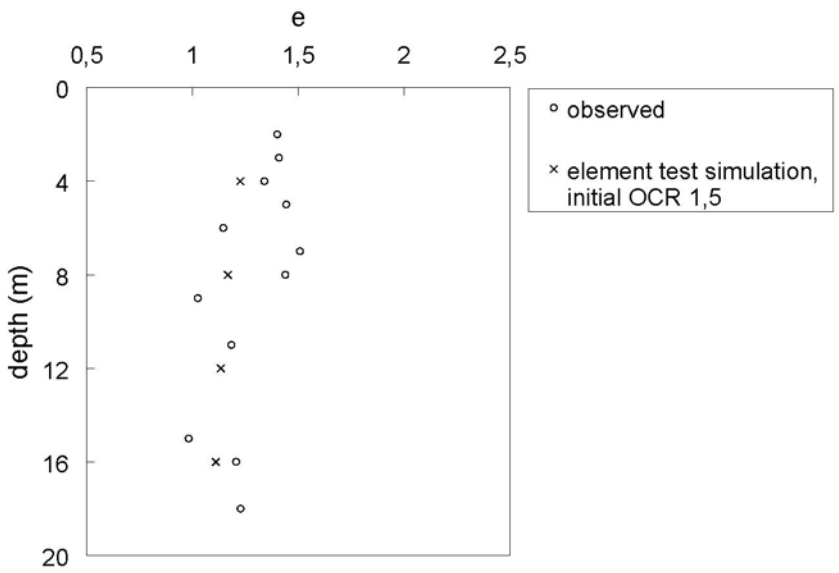

Fig. 6.10. Comparison of simulated initial void ratios, using an initial OCR of 1,5, with void ratios calculated from measured water content over depth.

It has to be mentioned that the measurements of water content on the soil samples from the borehole record, from which the void ratios were calculated, have no high accuracy and that the degree of saturation over depth was unknown. Therefore the observed void ratios have to be considered to be rather course indications. Considering this, Fig. 6.10 shows that an acceptable distribution of void ratio over depth could be achieved, using an initial OCR of 1,5. In many other geotechnical problems this appeared to be a realistic initial value as well (oral communication with Thomas Meier, 2005).

Fig. 6.11 shows the simulated velocities of slope movements for 1 m thick soil segments using a slope angle of 10° and the material parameters of Haselgebirge over a time-span of 18 years. The results are compared with the relative velocities calculated from the inclinometer measurements in B2 and B4, which were already shown in Fig. 5.9.

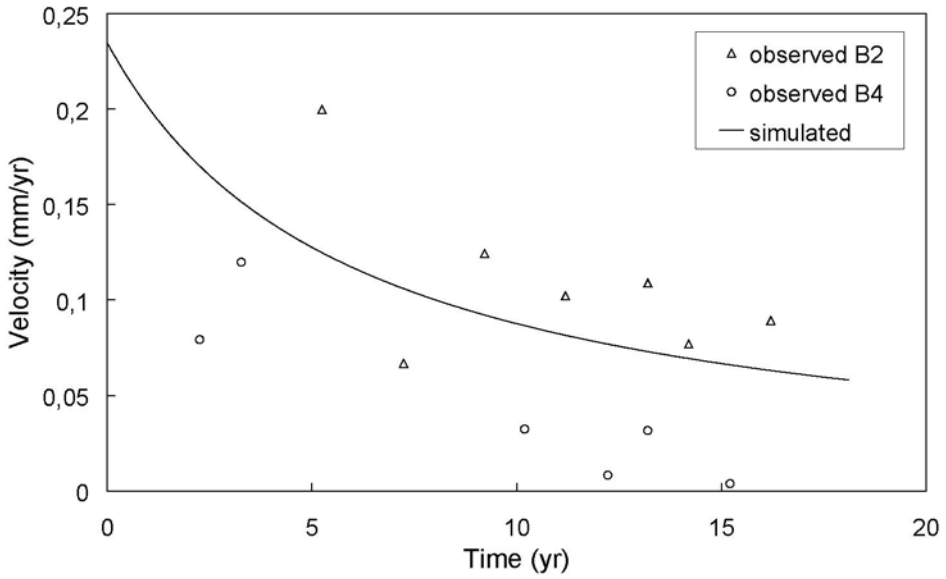

Fig. 6.11. Comparison between the simulated velocities of a 1 m thick slope section (averaged over simulated velocities at 4, 8, 12 and 16 m depth) and the relative velocities calculated from the inclinometer measurements in borehole B2 and B4, averaged over the total borehole length.

In order to test the impact of density on the velocity, slope movements were calculated at soil segments at four different depths: 4, 8, 12 and 16 m. The simulation results show that velocity is decreasing with depth, but only to a very small degree. At 16 m depth velocity is only around 0,6% smaller than at 4 m depth (after 12 years simulation)

6.5 Simulation of the slope deformations with a FE-model

In order to enable comparison between the results of the two models it was attempted to pose the boundary value problem for the FE-model as similar as possible to that posed for the element test model. The same material parameters and methods for determination of the initial state variables were used. The results of the presented FE-simulations can also be found in Van den Ham et al. (2005b).

6.5.1 FE-mesh and boundary conditions

As the spatial variability of the thickness of the slope body is relatively small (both in borehole B2 and B4 the bedrock surface was found at 20 m depth (Fig. 5.5)), the only slope geometric

parameter that significantly varies is slope angle. Therefore it was convenient to generate a relatively simple two-dimensional, plane-strain FE-mesh of a slope section, based on the subsurface model in Fig. 5.4. Merely by varying the slope angle, different locations of the slope could be simulated. Due to a lack of necessary information concerning the geometry beneath the location of the boreholes and the seismic profiles it was decided to leave out an extension of the model into three dimensions.

The slope section was considered to be a continuous ('solid') visco-hypoplastic body on a rigid bottom. In contrary to e.g. Cristescu et al. (2002), Desai et al. (1996) and Vulliet and Hutter (1988), no 'interface zone' (i.e. a zone in which the solid body can slip over the bedrock) was incorporated between the solid bottom and the basis, as the inclinometer measurements in the boreholes did not reveal the presence of a shear plane or shear zone (see Fig. 5.8 and Fig. 5.9). Nodes at the lower boundary of the mesh were constrained in both horizontal and vertical direction. The two side boundaries of the mesh could move freely but did undergo end stresses (which will be discussed in section 6.5.3).

Fig. 6.12 shows the final mesh geometry as well as the boundary conditions.
Simulations were performed with the FE-software Abaqus, Version 6.5-1 (Abaqus Inc, 2004).

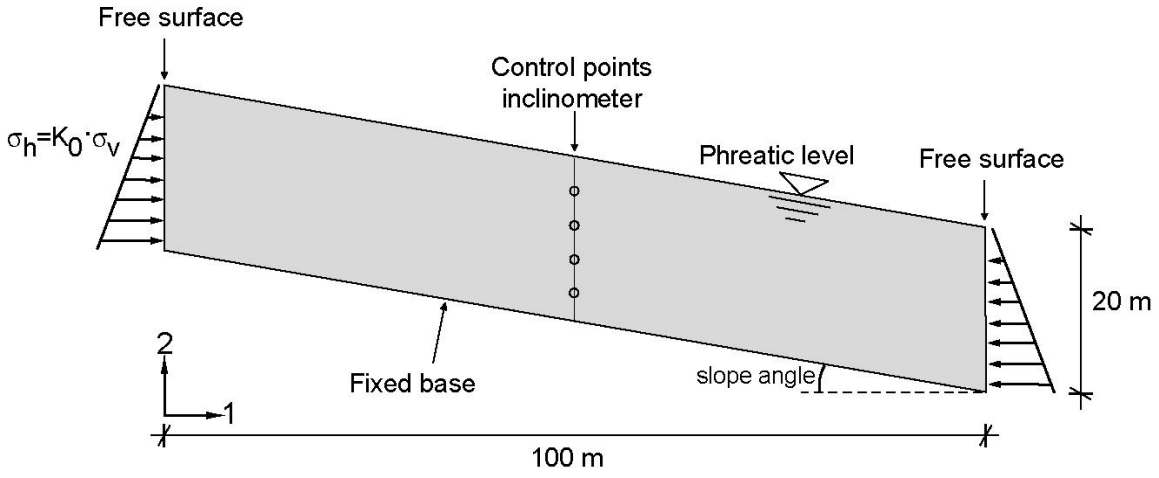

Fig. 6.12. Subsurface model, serving as a basis for the FE-model, with dimensions, boundary conditions, location of the inclinometer and location of four control points in which simulated and observed velocities were compared.

6.5.2 Initial state variables

The initial stresses in the FE-model at the free surfaces of the mesh' boundaries and within the mesh (i.e. vertical stresses and K_0) were calculated in an analogue manner as described in section 6.4.1, using the same densities and pore water pressure distribution (i.e. a phreatic level equal to the slope surface). Furthermore, completely drained conditions were assumed.

While K_0 is a variable within the mesh, at the side boundaries of the mesh this value had to be kept fixed. As it can be expected that during simulation K_0 increases over time due to relaxation (see section 3.5), this may have unwanted influences on the results. In order to reduce these as much as possible, the mesh was 'oversized' to a length of 100 m.

As mentioned in section 6.4.1, initial void ratio can either be set as an initial value or be calculated by the visco-hypoplastic law for a given OCR. As creep rate is strongly controlled by OCR, the effect of different initial OCR's on the initial void ratio distribution was studied by comparing this with the available measurements according to the method described in section 6.4.1.

For the same reasons as given in section 6.4.1, the first 6 years of simulation were left out in the comparison of the results with the observations.

6.5.3 Spatial and temporal discretisation

In order to investigate and minimise the dependence of the FE-calculations on spatial and temporal discretisation and to reduce calculation time as much as possible, the model was tested for its sensitivity to element size and maximal time increment. A smaller element size than 2×2 m did not yield improvements of the results. The maximum allowed time increment was determined to be $8 \cdot 10^5$ s. The FE-mesh consisted of four-noded isoparametric quadrilateral elements with four integration points. The final FE-mesh is shown in Fig. 6.13.

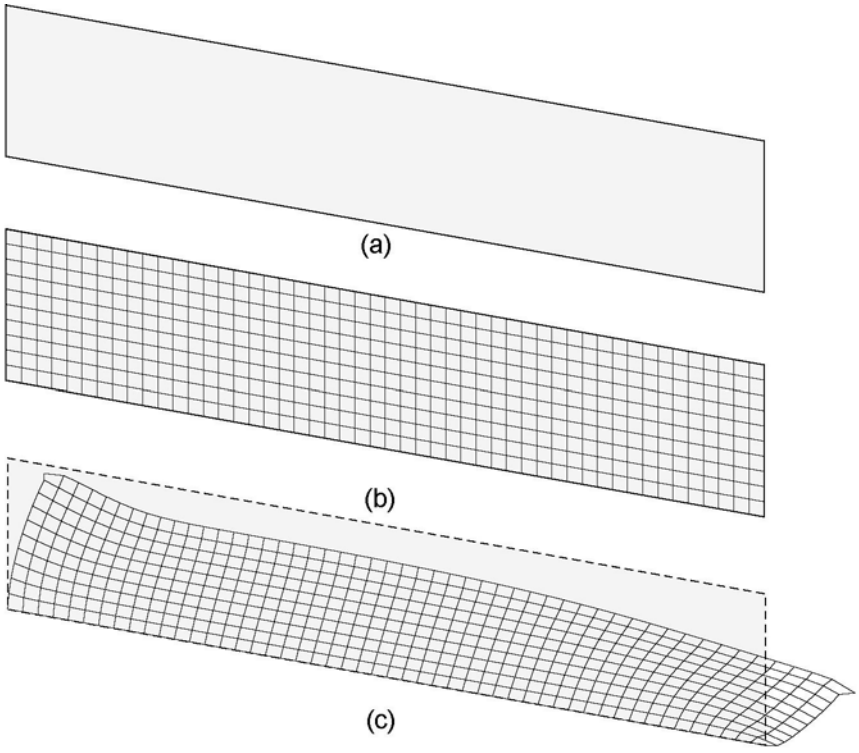

Fig. 6.13. Undeformed (b) and deformed (c) FE-mesh, based on the subsurface model (a and Fig. 6.12).

6.5.4 Results

Fig. 6.14 shows the observed and simulated decrease of void ratio (e) over depth and the influence of initial OCR. Increasing the initial OCR from 1,5 to 5 leads to a reduction of the void ratio of less then 0,1 for all depths. Considering the remarks given in section 6.4.2, also within the FE-mesh an acceptable initial void ratio could be obtained, using an initial OCR of 1,5. The obtained initial void ratio distribution is shown in Fig. 6.15.

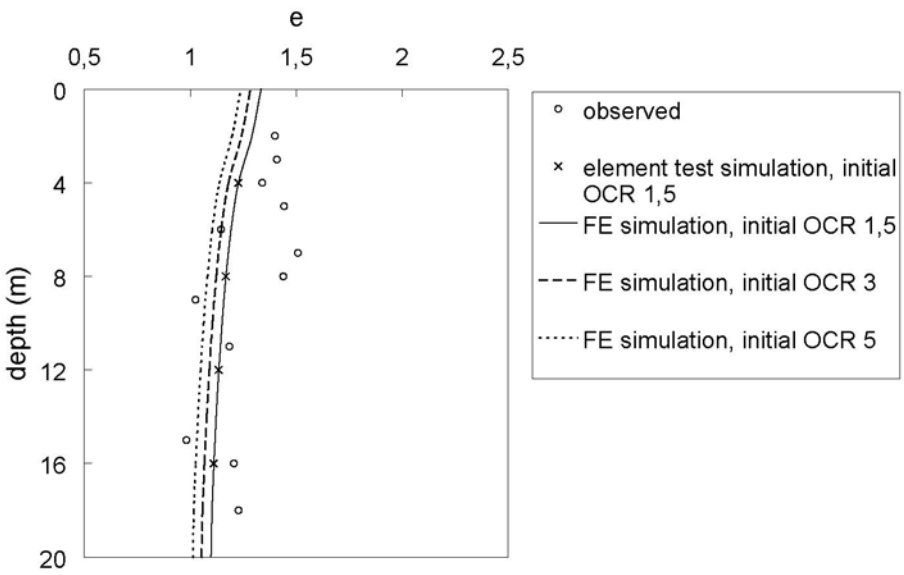

Fig. 6.14. Comparison of simulated initial void ratios (along a vertical cross section through the FE-mesh in Fig. 6.12) with void ratios calculated from measured water content over depth. Also the influence of different initial OCR's is shown.

Fig. 6.16 shows the results of the FE-simulations of the slope movements in both locations for a time-span of 18 years in a similar way as Fig. 6.11. Material parameters of Haselgebirge and a slope angle of 10° were used. Fig. 6.13(c) shows the deformed FE-mesh after 18 years (displacements have increased by a factor 50).

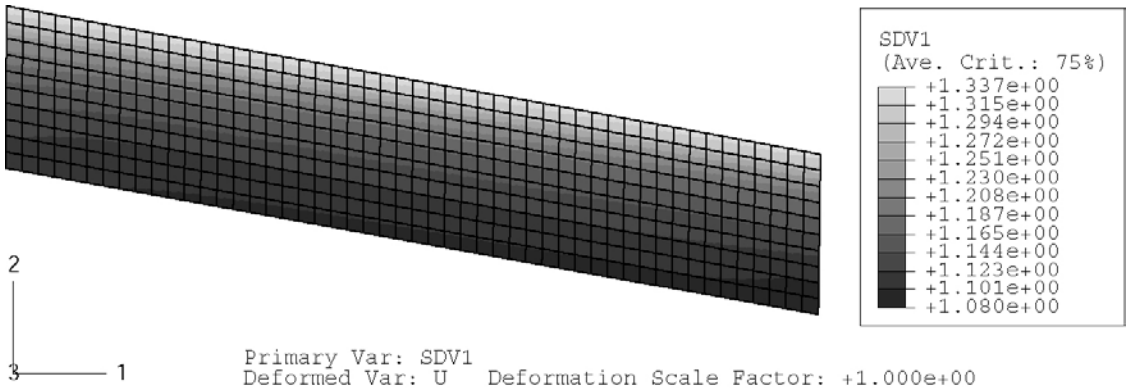

Fig. 6.15. Simulated initial void ratio ('SDV1') distribution if an initial OCR of 1,5 is used.

Only a small increase of relative velocity with depth was observed. After 10 years simulation, velocity at 4 m depth was around 3% lower than at 16 m depth. The depth-dependence tends to vanish over time.

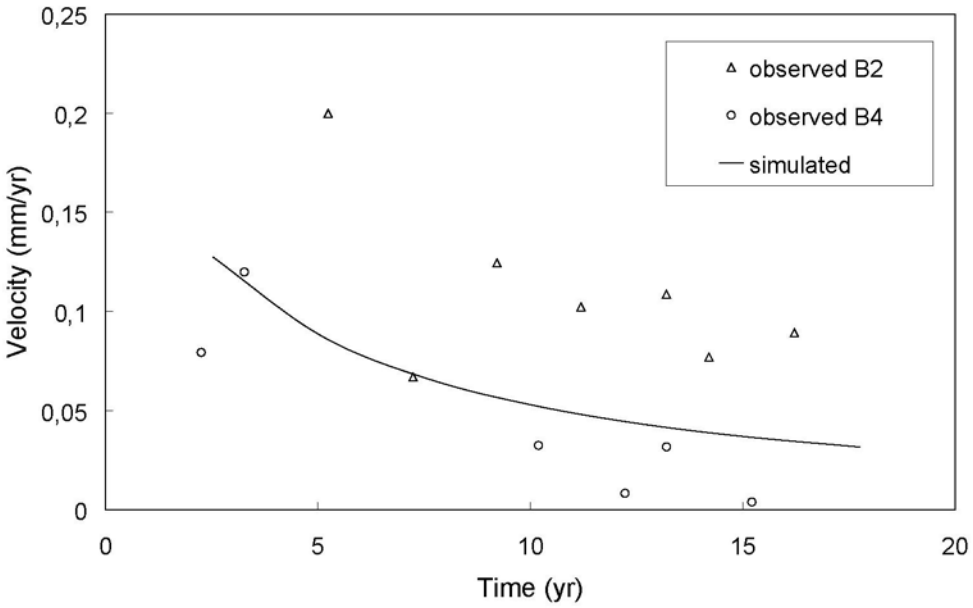

Fig. 6.16. Comparison between velocities simulated with the FE-method and observed velocities calculated from the inclinometer measurements, both averaged over the total borehole length.

6.6 Discussion

As explained in chapter 3, density and stress (which, together with deformation rate, determine OCR) strongly determine the viscous behaviour of the soil. Therefore, it is important to obtain a reasonable initial distribution of these variables. However, only initial density could be verified by field measurements. Fig. 6.10 and Fig. 6.14 show that a realistic initial distribution could be obtained with both models. For verification of the initial stress distribution no measurements were available at all. Theoretically, a realistic initial stress state could be obtained by simulating the complete stress history of the slope. However, in case of the Stambach slope, the available information of the history of the earth flow is insufficient and much too complex to reconstruct the slope history, as processes involved during activation and deactivation of the earth flow are largely unknown.

Fig. 6.11 and Fig. 6.16 show that for both models calculated velocities fit fairly well with the measured velocities and are approximately in between the velocities observed in the locations of B2 and B4. Velocities calculated with the element test model are closer to the measurements in

B2, whereas those calculated with the FE-method are closer to the measurements in B4. In section 6.6.2 some explanations will be given for these differences between the models.

An important result is that also the evolution of velocity over time could be simulated in an accurate way. Both simulations and observations show an approximately logarithmic deceleration of velocity (clearly visible if the trend lines in Fig. 5.10 are compared to simulated velocity-time curves).

The decreasing deformation rate can be explained by the proceeding densification of the slope materials over time, due to volumetric creep that accompanies deviatoric creep (which is possible due to drained conditions). This results in an increase of OCR, which, according to Eq. 3.8, leads to a decrease of the creep rate. The process of densification over time is illustrated in Fig. 6.17, showing the evolution of void ratio and OCR over time within the FE-mesh at two depths.

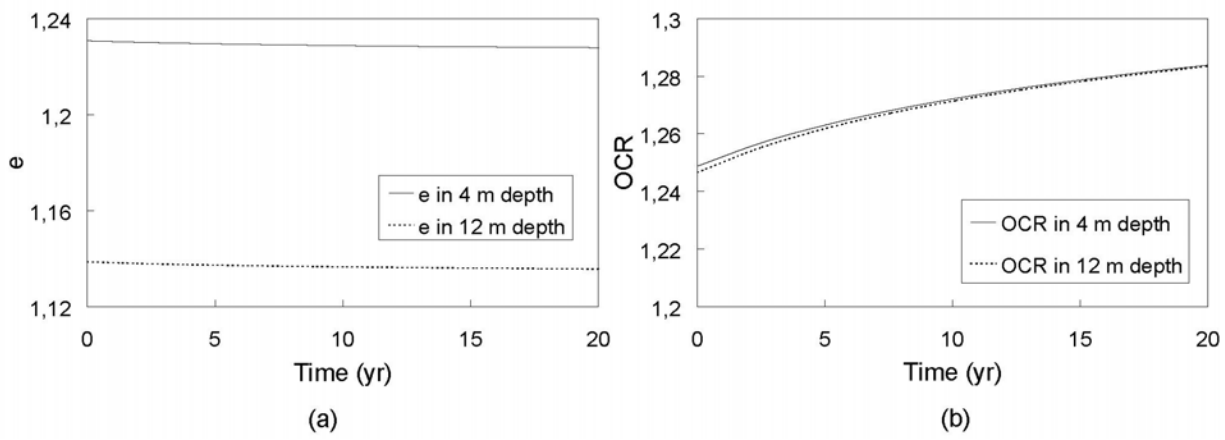

Fig. 6.17. Evolution of e (a) and OCR (b) over time at 4 and 12 m depth (results from FE-simulation).

On a microscopic level, the evolution of the slope movements can be explained as follows: densification due to volumetric creep leads to an increase of the total contact area between the soil particles. Consequently, the rate of densification is not constant, but decreases over time (i.e. the volumetric creep rate diminishes over time), as the stresses are kept constant or, in case of the FE-model, approximately constant.

Under the condition that applied stresses do not change and no excess pore water stresses develop, over very long time-spans OCR will reach asymptotically a stable value and therewith the slope movements as well. This means that the Stambach slope will eventually evolve into a stationary deforming slope (i.e. a constant creep rate).

Both element test and FE-simulations show that the influence of increasing density with depth is negligible. This is in agreement with the field observations in Fig. 5.8(b) and 5.9(b). Fig. 6.17(b) shows that OCR is nearly depth-independent as well.

6.6.1 Sensitivity analysis

An important issue with respect to the many assumptions and simplifications made in both the model approaches, is the sensitivity of the model to uncertainty. The extent to which estimation errors influence the model results needs to be assessed in order to make a final judgement of the applicability of the models.

The magnitude and distribution of the initial state variables, materials and pore water pressures within the slope body, and slope geometry used for the simulations, are all subject to uncertainties, which are a consequence of the strong heterogeneity of the slope materials and the sparse availability of measurements. The influence of these uncertainties on the model performance can approximately be quantified by means of sensitivity analyses, in which the unknown parameters and variables are varied between expected ranges. In this study the influence of a number of factors was quantified from which the maximum variability (i.e. the range) could be assessed from measurements or observations and from which the variability was expected to influence the model performance significantly. These are initial density, material parameters and distribution and slope angle. The influence of initial density was already shown in Fig. 6.10 and Fig. 6.14 and discussed in the corresponding sections. The latter two will be discussed in the following sections. Simplifications inherent to the models will be discussed in section 6.6.3.

6.6.1.1 Influence of material parameters and distribution

As explained in section 5.1 in the upper part of the slope both materials are found in unmixed form: the northwestern side predominantly consists of Haselgebirge, whereas the southeastern side mainly consists of Fleckenmergel. In a downhill direction they have been increasingly mixed. Therefore, the results as shown in Fig. 6.11 and Fig. 6.16 may hold at least for the upper

part of the slope, consisting of Haselgebirge. In principal, by comparing the simulation results using the material parameters of Haselgebirge to those using the parameters of Fleckenmergel, the maximum variation in velocities due to differences in material properties should be assessed.
Fig. 6.18 shows that for the element test model the relative velocities obtained using the Haselgebirge material parameters (and a slope angle of 10°) are approximately 1,8 times higher than those obtained with the Fleckenmergel parameters. This factor sustains over the complete simulation time. With the FE-model the velocities using Haselgebirge parameters are higher as well, but the difference with Fleckenmergel parameters increases from a factor 1,2 at the onset of the movements to a factor 1,3 after 18 years.

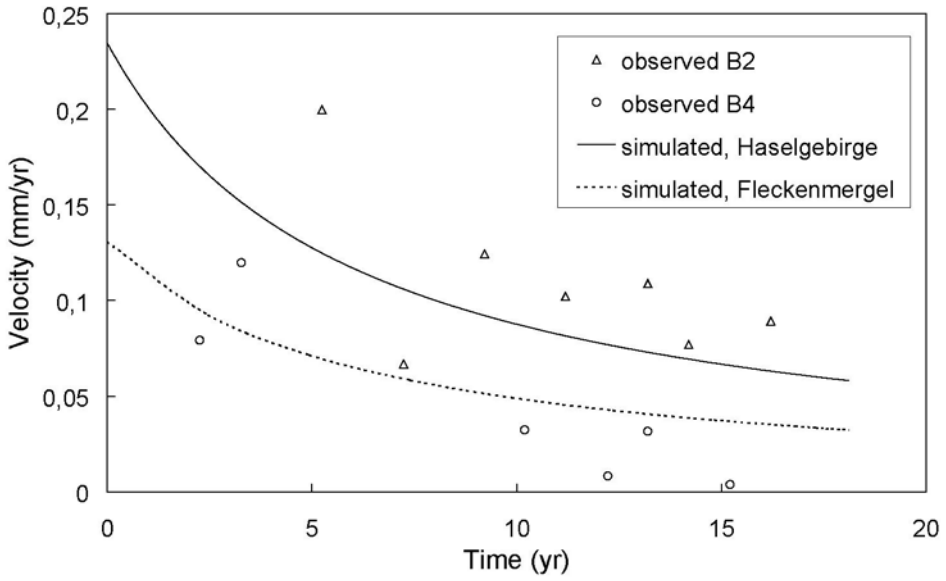

Fig. 6.18. Influence of material parameters on element test simulation results.

The higher creep rates in Haselgebirge can be ascribed to the smaller values of λ, κ and I_v (Table 6.1). Apparently the influence of the slightly larger critical friction angle φ_c, causing an increase of OCR, does not play a significant role.
It should again be emphasised that the Fleckenmergel samples, on which the material parameters were determined, did probably not represent the completely weathered material, of which the slide mass is expected mainly to consist of. Therefore stiffness and shear strength may have been overestimated, resulting in too low simulated deformation rates.

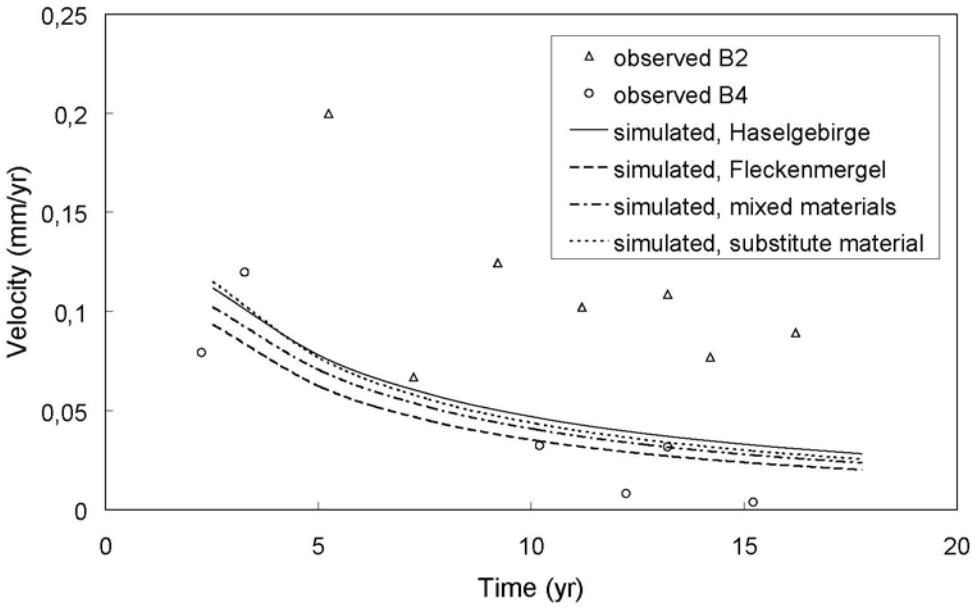

Fig. 6.19. Influence of material parameters on FE-simulation results.

Above the maximum variability of simulated creep velocities due to different material properties was quantified. In principal, simulation of any mixture of the materials should yield velocities somewhere in between. This was tested with the FE-method, in which, in contrary to the element test model, a heterogeneous material distribution can be accounted for. Data concerning the mode and degree of mixture of Haselgebirge and Fleckenmergel within the slope body were only available from the borehole records (Fig. 5.5). Although providing very detailed information in the location of the boreholes (on occasion showing a rapid alternation of materials, demonstrating the fine-scaled heterogeneity), they do not give insight into the spatial distribution of the materials in other locations of the slope. For this reason material distribution was approximated by assuming the materials to be mixed in equal proportions. The mixture was represented by means of the two methods that were discussed in section 3.4 and Fig. 3.6 and Fig. 3.7. The first method involves the assignment of the material parameters of Haselgebirge and Fleckenmergel to the individual elements according to a ‘checked pattern’, as shown in Fig. 6.19(a). Alternatively, heterogeneity was simulated by replacing the two materials by a single substitute material, in which the visco-hypoplastic parameters were averaged (Fig. 6.19(b)).

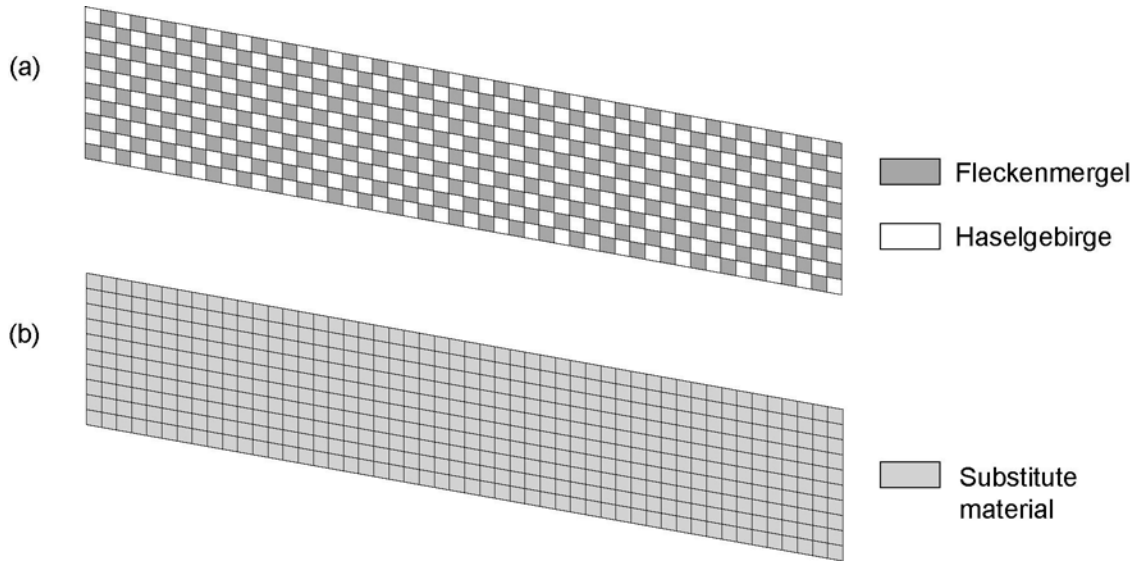

Fig. 6.20. FE-mesh using a 'checked pattern' material arrangement of Haselgebirge and Fleckenmergel (a) and using a substitute material (b).

Fig. 6.20 shows that the velocities, using a 'checked pattern' material distribution, exactly represent the average of the velocities obtained with Haselgebirge and Fleckenmergel material parameters. However, the evolution of velocities over time calculated with the substitute material deviates from the other curves. Obviously, the assumption of a linear relationship between slope deformation rate and the magnitude of each of the material parameters is not in agreement with the visco-hypoplastic equations. This makes a sensible interpretation of the results rather difficult. A more proper method for quantifying the influence of a mixture of both materials on the simulation results would be to determine the visco-hypoplastic parameters on a mixture prepared in the laboratory by means of the tests described in section 6.2. However, tests on mixtures were not conducted in this study.

6.6.1.2 Influence of slope angle

In section 5.4.1 the higher deformation rates in borehole B2 compared to those in borehole B4 were related to a higher slope inclination at that location. In the field it was observed that zones of contraction alternating with zones of distraction could be related to the local slope angle. This hypothesis was tested with the models by varying the slope angle between the maximum and

minimum observed values, which were determined to be 5° and 15°. The results are shown in Fig. 6.21 and Fig. 6.22 for the element test model and FE-model respectively.

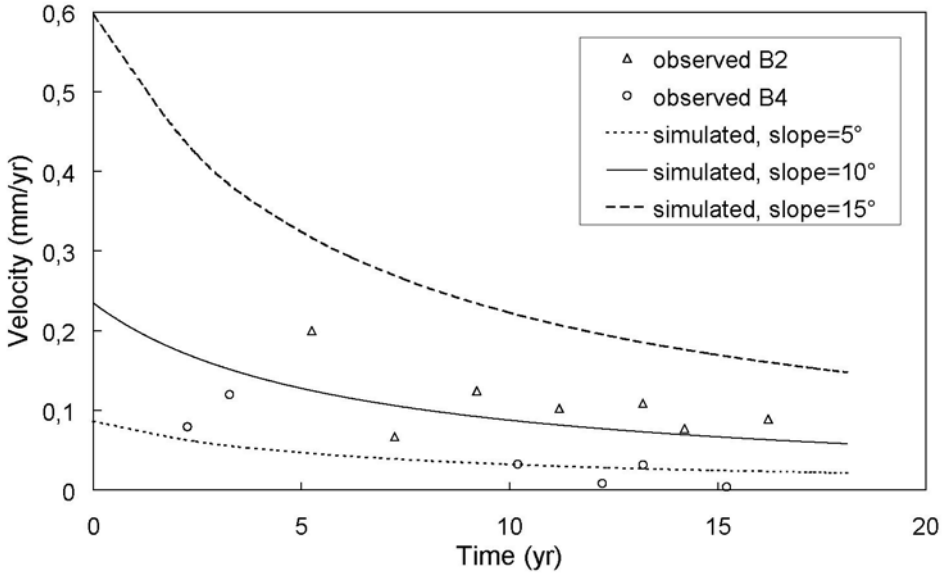

Fig. 6.21. Influence of slope angle on element test simulation results.

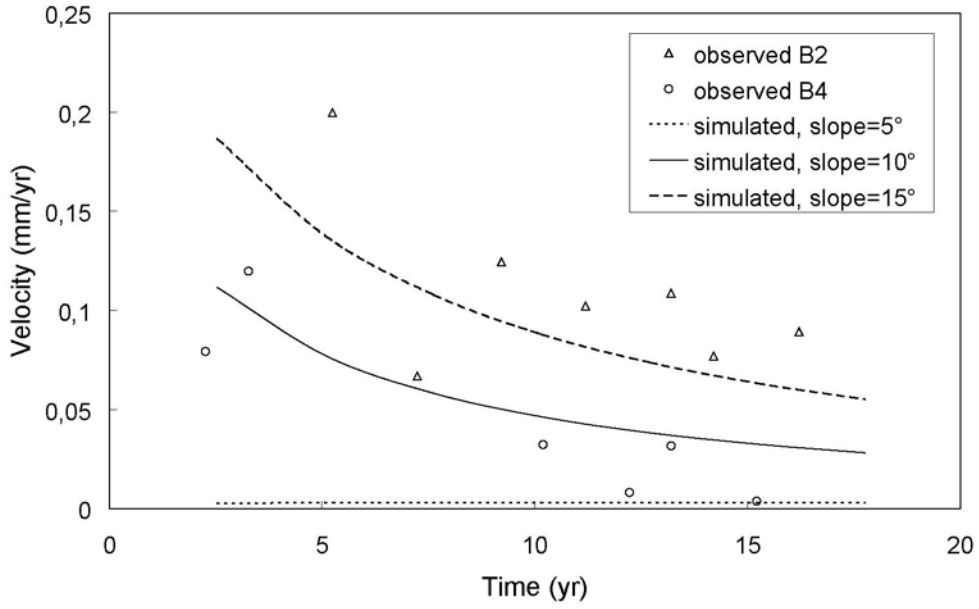

Fig. 6.22. Influence of slope angle on FE-simulation results.

In the element test model a reduction of the slope angle at 5° leads to an approximately 2,7 times lower deformation rate, whereas a slope angle of 15° results in an around 2,5 times higher deformation rate. Both times these factors sustain over the complete simulation time. With the

FE-model simulation of a 15° steep slope leads to an approximately 2,2 times higher velocity at the onset of the movements. After 18 years, this factor has increased to 1,7. Reduction of the slope angle at 5° immediately leads to a stationary creep rate of approximately 0,003 mm/yr.

The results show that with both models the variability in velocities observed in the locations of B2 and B4 can largely be covered by varying the slope angle between 5° and 15°. It should, however, be noticed that the influence of slope angle revealed by the model cannot be transmitted directly to the real slope, as in reality convexities and concavities of the slope profile down- and uphill of the slope section of interest also determine the slope movements. These confinements make that differences in velocities as a result of slope angle will be mitigated.

6.6.2 Comparison of the element test and FE-model

In the previous sections has already been indicated that the results obtained with the element test model deviate from those obtained with the FE-model. It appeared that the differences are not constant, but change over time and seem to be dependent on material parameters and slope angle. The differences can be quantified by calculation of the ratio between the velocities calculated with the element test model and those calculated with the FE-model, expressed by the factor *R*:

$$R = \frac{velocity_{elementtest\ \mathrm{mod}\ el}}{velocity_{FE-\mathrm{mod}\ el}} \qquad \text{(Eq. 6.1)}$$

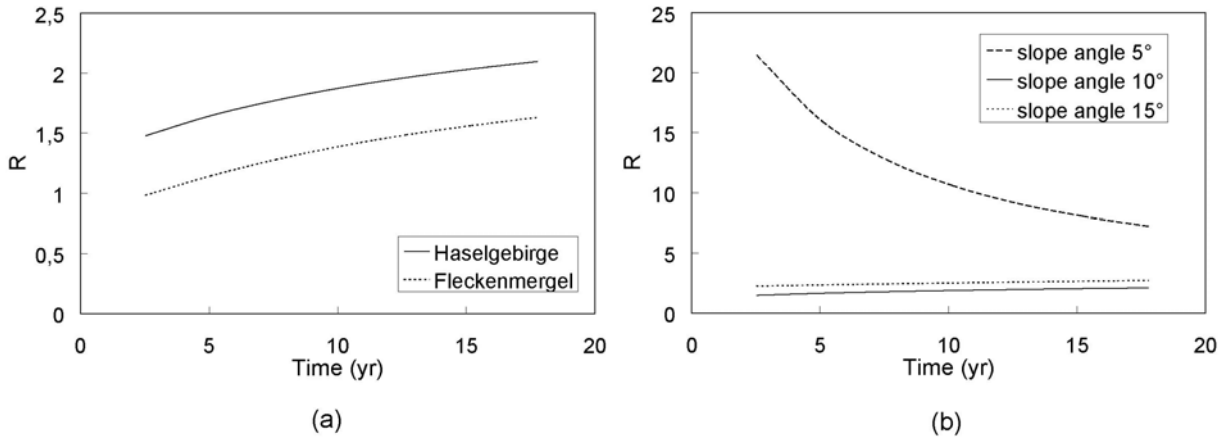

Fig. 6.23. Comparison between results of element test model and the FE-model.

Fig. 6.23 shows the evolution of *R* over time in relation to material parameters and slope angle. For all cases *R* is larger than 1, indicating that velocities obtained with the element test model are higher than those obtained with the FE-model. With material parameters of Haselgebirge the deviations are larger than with Fleckenmergel parameters. Also an increase of the slope angle to 15° results in a slight increase of *R*. A decrease of slope angle to 5°, however, leads to much higher velocities for the element test model, although the difference with the FE-model decreases over time.

The major difference between simulations conducted by the element test model and the FE-model is that within the element test model stresses are homogeneous and do not vary during simulation. In the FE-model only at the free surfaces of the side boundaries the ratio between horizontal and vertical stresses is fixed, whereas within the FE-mesh stresses are variable. Fig. 6.24 shows that vertical stresses and K_0 increase over time. As discussed in section 3.5 the latter may be explained by relaxation of the shear stresses. Since the stress state influences OCR, this also affects the slope deformation rates. This means that the fixed stresses within the element test model pose an important shortcoming of this approach and may largely explain its deviating results. The results of Fig. 6.24 further confirm the relevance of 'oversizing' of the FE-mesh, as the stress ratio at the side boundaries is fixed as well.

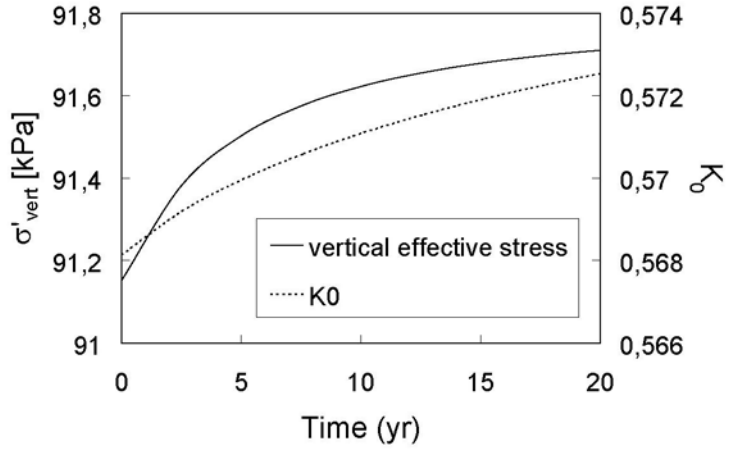

Fig. 6.24. Evolution of vertical effective stress and K_0 in the FE-mesh at 12 m depth.

Chapter 7 Conclusions

The objective of this study was to test the applicability of the visco-hypoplastic material law (in the version of Niemunis (2003)) for the prediction of creep movements of a large-size natural slope in the Upper-Austrian Alps. The material law has been validated for many geotechnical problems, but application to a large-size natural slope was not been done before. This study showed that with the applied methodology the creep movements could be simulated realistically. In this chapter the results are summarised and discussed. Furthermore, on the basis of the findings of this study, some recommendations with respect to application of the material model for prediction of other large-size natural slopes are given.

7.1 Summary

In Part 1 of this thesis the microscopic aspects of the (viscous) deformation behaviour of cohesive soils, together with its description by the visco-hypoplastic material law, were discussed. The visco-hypoplastic material law describes important properties such as relaxation, creep and rate-dependence in an accurate manner and was already validated for many geotechnical problems. A major advantage of this material law is that required material parameters, which are strictly separated from state variables, can be determined with ordinary laboratory tests (i.e. oedometer and triaxial tests). However, if applied on complex geotechnical problems such as large-size creeping slopes, the validity of the material law only partly determines the quality of model outcomes. Just as important for the predictive quality of the model is the availability of subsurface model, which should be able to provide a realistic representation of the driving and controlling factors and parameters, such as the magnitude and distribution of the material parameters, the initial state variables (density and stress), the pore water pressure distribution and the slope geometry.

Subsurface information on large slopes, however, is generally only available to a limited extent. Possibilities to obtain such data are limited as slope materials are generally very heterogeneous while limitations in time and costs do not allow for extensive sampling. In-situ measurements of stresses and densities are often not available at all. On the other hand, the very fine-scaled

information provided by borehole records can often not be incorporated in the model completely, as this would make the model too complex.

All this means that compromises with respect to the representation of the above mentioned parameters and variables are inevitable. These compromises concern homogenisation of material heterogeneities and slope geometry and assumptions with respect to initial state variables and boundary conditions for which measurements are often lacking completely. In chapter 3 two methods for homogenisation of material heterogeneity of complex subsurface models were given: joining of many thin layers into larger zones and replacement of many thin layers with different properties by a single substitute material.

In Part 2 the visco-hypoplastic material model and the described methods for dealing with limited availability of subsurface data were applied and tested on a natural creeping slope in Upper-Austria. The available data were (a) six borehole records and three seismic profiles, (b) three long-term inclinometer measurements (revealing deformation rates to be homogeneous over depth and to decrease over time), (c) free water tables in the inclinometer boreholes, (d) pore water pressures at three different depths at three locations, and (e) two samples from which visco-hypoplastic material parameters were determined by means of laboratory tests.
The validity of the material law for describing the behaviour of the slope materials was verified by simulating the laboratory element tests on the samples (in which the material properties were known to be homogeneous). By means of these laboratory tests the visco-hypoplastic material parameters were obtained. In chapter 4 and 5 the distribution of slope materials, slope geometry, as well as the distribution of pore water pressure and density was determined, based on a combination of measurements and geological and geomorphological expertise. Based on geological and geomorphological mapping, it could be deduced that the slope consists of two different source materials, which in the lower parts of the slope have been mixed. Therefore the two samples were taken from the unmixed materials for determination of the visco-hypoplastic material parameters. This way their maximum variability could be assessed.

Chapter 6 showed the simulation of the slope deformations, using a relatively simple element test model and a FE-model of two-dimensional slope sections. Compared to the FE-model, the

element test model is easier to design and calculation times can be kept relatively short. The aim of using different models was to test to what extent the simplifications of the element model compared to the FE-model affected the predictive quality of the model. By using the same set of material parameters, initial state variables, pore water pressure distribution and slope geometry for the two models, the simulation results could be compared which each other. The simplifications of the element test model involve the homogeneous distribution of material parameters and state variables and the invariability of stresses. The limitation of the homogeneous material distribution could largely be overcome by using small elements of 1 m. Fields of deformation rate could then be analysed by simulating slope segments at different depths. However, the invariability of stresses imposed by the element test model is not realistic and conflicts with visco-hypoplasticity. This presumably explains the differences between results obtained with the element test model and the FE-model, which does not suffer these shortcomings. It was shown that, depending on material parameters and slope angle, the velocities calculated with the element test model were up to two times higher than those obtained with the FE-model (except for a very small slope angle, when the difference was much bigger).

By means of sensitivity analyses the influence of the compromises (i.e. uncertainty on estimations of material parameters and distribution and slope angle) on the model results was quantified. This way also differences in deformation rates at different locations of the slope could be explained.

The maximum variation of deformation rate due to different material parameters was assessed, using the material parameters of the unmixed source materials for the whole complete model. Material parameters were found to change the simulated velocity by a factor 1,8 and 1,2-1,3 for the element test model and FE-model respectively. In principal, any mixture of both materials should yield velocities in between. With the FE-model a heterogeneous material distribution was simulated (using a FE-mesh having a ‘checked pattern’ material assignment), which proved the relation between material mixture and deformation rate to be proportional. An alternative (and possibly better) method for quantifying the influence of material heterogeneity would be to determine material properties at mixtures prepared in the laboratory.

An increase of the slope angle with 5° resulted in 2,5 and 2,2-1,7 times higher velocities for the element test model and FE-model respectively. A decrease of slope angle with the same amount led to a 2,7 times lower velocity for the element test model, whereas for the FE-model immediately stationary creep was obtained. It should, however, be mentioned that, due to the simplified model geometry, the influence of changes of *mean* slope angle were tested, whereas in reality slope angle is only a variable *within* the slope, expressed by a sequence of concavities and convexities. Realistic simulation is only possible using a more complex FE-mesh geometry in which local variations of slope geometry can be incorporated.

7.2 Applications and recommendations

So far, this study has demonstrated the applicability of the visco-hypoplastic law for predicting the creep movements of large-size natural slopes consisting of cohesive and completely saturated materials. However, it has to be emphasised that for the slope studied a relatively extensive data set was available and created, involving both in-situ measurements as well as laboratory data, which is for a slow moving slope a rather unique situation. Therefore, the question arises to what extent the material law can also be applied to other slopes, for which less subsurface data are available.

The visco-hypoplastic material law requires information on material parameters and initial values for stress and density. Therefore within the slope their magnitude and distribution have to be assessed. Based on the findings of this study, in which the influence of simplifications (e.g. homogenisation) and assumptions concerning above factors on the quality of the simulation were investigated, it can be concluded that with the visco-hypoplastic law sound results can be obtained, serving as a basis for prediction, only by a combination of measurements (in-situ as well as laboratory experiments) and a profound (engineering) geological knowledge of the slope studied. These include:

- determination of the dimensions (length and width) and type of the slope movements by means of engineering geological investigations.
- in order to determine the slope materials and their spatial distribution, the source materials of the deforming slope have to be identified and the slope historical evolution has to be

reconstructed. This requires a thorough (engineering) geological understanding of the slope studied as well as its source areas.

- based on the previous point, few samples have to be taken that comprise the variability within the slope. From these samples visco-hypoplastic material parameters can be determined using the methods used in this study. However, critical friction angle can also be (indirectly) determined by means of less expensive direct shear box tests, whereas I_v can also be estimated from the liquid limit using the empirical relation of Eq. 3.16.
- information about the thickness of the deforming mass and slope angle of the basis of the slide mass is crucial. At least one borehole logging, with which the unmoved basis is reached, should be available. Inclinometer measurements (which can be performed in the borehole) are required to assess the distribution of the movements with depth (e.g. the presence of possible shear zones should be accounted for in the model). In case no further spatial information concerning the basis of the deforming body is available, for slopes having a small thickness/length ratio, the basis can be assumed to run approximately parallel with the slope surface (similar to the slope studied).
- information concerning the pore water pressure distribution is required. If piezometer measurements are lacking, a phreatic surface equal to the free water table in the borehole can be incorporated in the model. It should also be accounted for seasonal variations, which may be considerable.
- an indication of density distribution is required, which can be obtained by determining the water content at borehole material from different depths (in case borehole logging was performed with core recovery).

Considering the above list, the question may rise to what extent numerical simulation provides additional predictive value to the measurements already performed. Using the case study as an example, one might say that slope movements can also be predicted simply by extrapolation of the inclinometer results. However, the fact that the material law has proven its validity for describing the mechanical behaviour of cohesive soils (not only under drained conditions and without changes of boundary conditions, as is the case in this study), combined with the findings of this study (i.e. that with simplifications and assumptions concerning distribution of material parameters, initial stress variables, pore water pressure and slope geometry slope deformations

can be simulated realistically), suggests that the method may also be applicable for more complex slides in which prediction cannot be based on the simple extrapolation of the measurements. With respect to the slope studied here, this implies that the material law may for example be used for studying the effect of the development of excess pore water pressures due to a rock fall event (see chapter 5). With respect to other slopes, this means that the model can be used for analysing different scenarios causing changes of the stresses within the slope and therewith slope deformation. This may involve the influence of constructions or analysis of stabilisation measures (e.g. retaining structures, modifications of the slope profile or drainage).

Therefore, although the results presented in this thesis may not appear to be very spectacular by themselves, a first step in verifying the applicability of the visco-hypoplastic material law to large, complex, slow-moving landslides has been made. The results encourage further research on the applicability of the material law to even more complex landslides, in order to, eventually, enable the application of this law for predictions of landslide behaviour and therewith disaster-prevention.

References

Abaqus Inc., 2004. Abaqus Version 6.5 Online Documentation.

Bathe, K.J., 1990. Finite-Elemente-Methoden. Springer-Verlag, Berlin.

Borja, R.I., Wren, J.R., 1996. Micromechanics of granular media. 1. Generation of overall constitutive equations for assemblies of circular disks. Computer Methods in Applied Mechanics and Engineering 127 (1-4), 13-36.

Collins, K., McGown, A., 1974. The form and function of microfabric features in a variety of natural soils. Géotechnique 24 (2), 223-254.

Cristescu, D.D., Cazacu, O., Cristescu, C., 2002. A model for slow motion of natural slopes. Canadian Geotechnical Journal 39 (4), 924-937.

Cruden, D.M., Varnes, D.J., 1996. Landslide types and processes. In: Turner, A.K., Schuster, R.L. (Eds.), Landslides: Investigation and Mitigation, Special Report 257, Transportation Research Board, National Research Council, National Academic Press, pp. 36-75.

Cundall, P., Strack, O., 1979. A discrete numerical model for granular assemblies. Géotechnique 29, 47-65.

Desai, C.S., Samtani, N.S., Vulliet, L., 1995. Constitutive Modelling and Analysis of Creeping Slopes. Journal of Geotechnical Engineering 121 (1), 43-56.

Duncan, J.M., 1996. State of the Art: Limit Equilibrium and Finite-Element Analysis of slopes. Journal of Geotechnical Engineering 122 (7), 577-595.

Eisbacher, G.H., 1996. Einführung in die Tektonik. Ferdinand Enke Verlag, Stuttgart.

Fernandez-Steeger, T., 2002. Erkennung von Hangrutschungssystemen mit Neuronalen Netzen als Grundlage für Georisikoanalysen. Ph.D. thesis. Department of Applied Geology, University of Karlsruhe.

Gudehus, G., 1981. Bodenmechanik. Ferdinand Enke Verlag, Stuttgart.

Gudehus, G., 1996. A comprehensive constitutive equation for granular materials. Soils and Foundations 36 (1), 1-12.

Gudehus, G., 2003. Ratcheting und DIN 1054. Mitteilungen des Institutes und der Versuchsanstalt für Geotechnik der TU Darmstadt, Vol. 64, 159-172.

Gudehus, G., 2003. Visco-hypoplasticity and observational method for soft ground. In: Natau,O., Fecker, E., Pimentel, E. (Eds.), Geotechnical Measurements and Modelling, A.A. Balkema Publishers, Lisse, pp. 169-179.

Herle, I., 1997. Hypoplastizität und Granulometrie einfacher Korngerüste. Ph.D. thesis, Veröffentlichungen des Institutes für Bodenmechanik und Felsmechanik, Vol. 142, University of Karlsruhe.

Hill, R., 1998. The mathematical theory of plasticity. University Press, Oxford.

Hutchinson, J.N., Bhandari, R.K., 1971. Undrained loading – a fundamental mechansim of mudflows and other mass movements. Géotechnique 21, 353-358.

Karcher, C., 2003. Tagebaubedingte Deformationen im Lockergestein. Ph.D. thesis, Veröffentlichungen des Institutes für Bodenmechanik und Felsmechanik, Vol. 160, University of Karlsruhe.

Kolymbas, D., 1998. Geotechnik-Bodenmechanik und Grundbau. Springer-Verlag, Berlin.

Krieg, S., 2000. Viskoses Bodenverhalten von Mudden, Seeton und Klei. Ph.D. thesis, Veröffentlichungen des Institutes für Bodenmechanik und Felsmechanik, Vol. 150, University of Karlsruhe.

Leinenkugel, H.J., 1976. Deformations- und Festigkeitsverhalten bindiger Erdstoffe; Experimentelle Ergebnisse und ihre physikalische Bedeutung. Ph.D. thesis, Veröffentlichungen des Institutes für Bodenmechanik und Felsmechanik, Vol. 66, University of Karlsruhe.

Mandl, G.W., 2000. The Alpine sector of the Tethyan shelf - Examples of Triassic to Jurassic sedimentation and deformation from the Northern Calcareous Alps.- Mittl. Österr. Geol. Ges. 92, 61-77.

Medwenitsch, W., 1957. Die Geologie der Salzlagerstätten Bad Ischl und Alt-Aussee (Salzkammergut). Mitteilungen der Geologischen Gesellschaft Wien 50, 137-199.

Mitchell, J.K., 1993. Fundamentals of soil behaviour. John Wiley & Sons, New York.

Moser, M., Meier, H., Lotter, M., Weidner, S., 2002. Geotechnical aspects of deep-seated mass movements in Austria. In: Rybar, J., Semberk, J., Wagner, P. (Eds.), Landslides, A.A. Balkema Publishers, Lisse, pp. 423-429.

Niemunis, A., Krieg, S., 1996. Viscous Behaviour of Soil Under Oedometric Conditions. Canadian Geotechnical Journal 33, 159-168.

Niemunis, A., 1996. A visco-plastic model for clay and its FE-implementation. Resultats recents on méchanique des sols et des roches, XIth Colloque Franco-Polonais, Gdansk, 151-162.

Niemunis, A., 2003. Extended hypoplastic models for soils. Dissertation for habilitation, Schriftenreihe des Instituts für Grundbau und Bodenmechanik, Vol. 34, University of Bochum, Germany.

Norton, F., 1929. The creep of steel at high temperatures. McGraw Hill Book Company Inc., New York.

Nübel, K., 2002. Experimental and Numerical Investigation of Shear Localization in Granular Material. Ph.D. thesis, Veröffentlichungen des Institutes für Bodenmechanik und Felsmechanik, Vol. 159, University of Karlsruhe.

Nübel, K., Karcher, C., 1998. FE Simulations of granular material with a given frequency distribution of voids as initial condition. Granular Matter 1, 105-112.

Persson, B.N.J., 1995. Theory of friction: stress domains, relaxation, and creep. Physical Review B 51 (19), 13568-13585.

Plöchinger, B., 1982. Erläuterungen zu Blatt 95 Sankt Wolfgang im Salzkammergut. Geol. B.-A. Wien, Wien.

Prevost, J.H., Popescu, R., 1996. Constitutive Relations for Soil Materials. The Electronic Journal of Geotechnical Engineering 1.

Rohn, J., 1991. Geotechnische Untersuchungen an einer Großhangbewegung in Bad Goisern (Oberösterreich). Ph.D. thesis, Schriftenreihe Angewandte Geologie, Vol 14, University of Karlsruhe.

Rohn, J., Czurda, K., Zvelebil, J., Zika, P., 1996. A steep wall with toppling rockpillars on a clayey subsoil. In: Chacón, J., Irigaray, C., Fernández, T. (Eds.), Landslides, A.A. Balkema Publishers, Rotterdam, pp. 181-188.

Rohn, J., Resch, M., Schneider, T., Fernandez-Steeger, T.M., Czurda, K., 2004. Large-scale lateral spreading and related mass movements in the Northern Calcareous Alps. Bulletin of Engineering Geology and the Environment 63, 71-75.

Roscoe, K.H., Burland, J.B., 1968. On the Generalized Stress-Strain Behaviour of Wet Clay. In: Heyman, J., Leckie, F.A. (Eds.), Engineering Plasticity, Cambridge University Press, Cambridge, pp. 535-609.

Samtami, N.C., Desai, C.S., Vulliet, L., 1996. An interface model to describe viscoplastic behavior. International Journal of Numerical and Analytical Methods in Geomechanics 20 (4), 231-252.

Schäffer, G., 1976. Einführung zur Geologischen Karte der republik Österreich, Blatt 96, Bad Ischl. In: Gattinger, T. et al. (Eds.), Arb. Tag. Geol. B.-Anst. Wien, Salzkammergut, pp. 6-26.

Schäffer, G., 1982. Geologische Karte der Republik Österreich, Sheet 96 Bad Ischl (1:50 000), Wien.

Schäffer, G., 1983. Die aktuelle Massenbewegung Stambach-Zwerchwand/Bad Goisern. Arb. Tag. Geol. B.-Anst. Wien, 28-29.

Schauberger, O., 1978. Die alpinen Salzlagerstätten. Verh. Geol. B. A. 3, 455-459.

Schofield, A., Wroth, C.P., 1968. Critical State Soil Mechanics. McGraw-Hill, London.

Tollmann, A., 1976. Analyse des klassischen nordalpinen Mesozoikums. In: Monographie der Kalkalpen, Vol. 2. Deutlicke Verlag, Wien.

Van den Ham, G., Rohn, J., Meier, T., Czurda, K., 2005a. A method for modeling of a creeping slope with a visco-hypoplastic material law. Accepted by Mathematical Geology.

Van den Ham, G., Rohn, J., Meier, T., Czurda, K., 2005b. Finite element simulation of a slow moving natural slope in the Upper Austrian Alps using a visco-hypoplastic law. Submitted to Geomorphology.

Van Husen, D., 1977. Zur Fazies und Stratigraphie der jungpleistozänen Ablagerungen im Trauntal. Jahrbuch der Geolischen Bundesanstalt, Vol. 120 (1), Wien, 1-130.

Varnes, D.J., 1978. Slope movement and types and processes. In: Schuster, R.L., Krizek, R.J. (Eds.), Landslides: Analysis and Control. Transportation Research Board, National Academy of Science, Special report 176, Washington DC, pp. 11-33.

Vulliet, L., Hutter, K., 1988. Continuum model for natural slopes in slow movement. Géotechnique 38 (2), 199-217.

Weigert, U., 1971. Zur Geologie der Hallstätter Zone östlich Bad Goisern (Oberösterreich). Ph.D. thesis, University of Vienna.

Wilson, A., Petley, D., Murphy, W., 2003. Down-slope variation in geotechnical parmeters and pore fluid control on a large-scale Alpine landslide. Geomorphology 54, 49-62.

Xiang, W., 1997. Der Einfluß der Kationenbelegung auf die bodenmechanischen und rheologischen Eigenschaften von Tonen am Beispiel einer ostalpinen Großhangbewegung. Ph.D. thesis, Schriftenreihe Angewandte Geologie, Vol. 48, University of Karlsruhe.

Yoshida, T., Tatsuoka, F., Siddiquee, M., Kamegai, Y., Park, C.S., 1974. Shear banding in sands observed in plain strain compression. In: Chambon, R., Desrues, J., Verdoulakis, I. (Eds.), Localization and bifurcation theory for soils and rocks, A.A. Balkema Publishers, Lisse, pp. 165-179.